AEROSPACE REPORT NO.
TR-2009(8550)-2

Particle Deposition onto Enclosure Surfaces

20 August 2009

De-Ling Liu
Space Materials Laboratory
Physical Sciences Laboratories

Prepared for:

Space and Missile Systems Center
Air Force Space Command
483 N. Aviation Blvd.
El Segundo, CA 90245-2808

Authorized by: Engineering and Technology Group

This report was submitted by The Aerospace Corporation, El Segundo, CA 90245-4691, under Contract No. FA8802-09-C-0001 with the Space and Missile Systems Center, 483 N. Aviation Blvd., El Segundo, CA 90245. It was reviewed and approved for The Aerospace Corporation by G. F. Hawkins, Principal Director, Space Materials Laboratory; and D. C. Marvin, Principal Director, Research and Program Development Office. Col. David E. Swanson was the project officer for the Mission-Oriented Investigation and Experimentation (MOIE) program.

This report has been reviewed by the Public Affairs Office (PAS) and is releasable to the National Technical Information Service (NTIS). At NTIS, it will be available to the general public, including foreign nationals.

This technical report has been reviewed and is approved for publication. Publication of this report does not constitute Air Force approval of the report's findings or conclusions. It is published only for the exchange and stimulation of ideas.

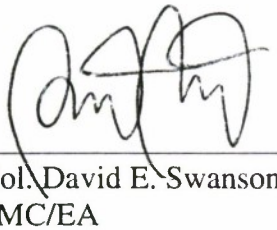

Col. David E. Swanson
SMC/EA

REPORT DOCUMENTATION PAGE

Form Approved
OMB No. 0704-0188

1. REPORT DATE (*DD-MM-YYYY*)	2. REPORT TYPE	3. DATES COVERED *(From - To)*
20-08-2008		

4. TITLE AND SUBTITLE

Particle Deposition onto Enclosure Surfaces

5a. CONTRACT NUMBER
FA8802-09-C-0001

5b. GRANT NUMBER

5c. PROGRAM ELEMENT NUMBER

6. AUTHOR(S)

De-Ling Liu

5d. PROJECT NUMBER

5e. TASK NUMBER

5f. WORK UNIT NUMBER

7. PERFORMING ORGANIZATION NAME(S) AND ADDRESS(ES)

The Aerospace Corporation
Physical Sciences Laboratories
El Segundo, CA 90245-4691

8. PERFORMING ORGANIZATION REPORT NUMBER

TR-2009(8550)-2

9. SPONSORING / MONITORING AGENCY NAME(S) AND ADDRESS(ES)

Space and Missile Systems Center
Air Force Space Command
483 N. Aviation Blvd.
El Segundo, CA 90245

10. SPONSOR/MONITOR'S ACRONYM(S)
SMC

11. SPONSOR/MONITOR'S REPORT NUMBER(S)

12. DISTRIBUTION/AVAILABILITY STATEMENT

Approved for public release; distribution unlimited.

13. SUPPLEMENTARY NOTES

14. ABSTRACT

In space applications, the main concern of particle deposition arises from the undesirable effects of surface obscuration on contamination-sensitive surfaces. The development of effective mitigation strategies to minimize particulate contamination requires the understanding of particle transport and deposition as well as the associated physical factors affecting the processes. The knowledge gleaned from the state-of-the-art literature review presented here can be applied to an enclosure scale as small as a spacecraft payload cavity, or as large as a clean room in a manufacturing/processing facility. The insights from studying the physical processes that influence the rate of particle deposition within an enclosure are expected to provide a strong scientific foundation to benefit various aspects of aerospace contamination control needs.

15. SUBJECT TERMS

Particle deposition, Particle transport, Particulate contamination

16. SECURITY CLASSIFICATION OF:			17. LIMITATION OF ABSTRACT	18. NUMBER OF PAGES	19a. NAME OF RESPONSIBLE PERSON
					De-Ling Liu
a. REPORT	b. ABSTRACT	c. THIS PAGE			19b. TELEPHONE NUMBER *(include area code)*
UNCLASSIFIED	UNCLASSIFIED	UNCLASSIFIED		58	(310)336-0062

Acknowledgments

This work was supported under The Aerospace Corporation's Mission Oriented Investigation and Experimentation program, funded by the U.S. Air Force Space and Missile Systems Center.

The author thanks Professor William W Nazaroff at UC Berkeley for providing valuable comments.

Contents

Figures

Tables

1. Introduction

The study of particle deposition from aerosol flow onto surfaces in enclosed spaces has attracted considerable attention in the past few decades owing to its significance in a great variety of technological applications, such as microcontamination control in the semiconductor industry,[1,2] aerosol production in chemical reactors,[3] indoor air pollution,[4–6] and soiling of artworks,[7] as well as nuclear reactor safety analysis.[8,9] Both desirable and undesirable outcomes may result from the processes of particle deposition. For instance, the thin-film coating techniques used to generate unique surface properties are an application of the desirable outcome.[10,11] In contrast, there are many examples of undesirable particle deposition, which causes surface contamination or even material damage. One of the well-known examples is the reduced yield of integrated circuits in the wafer manufacturing process. Particulate contamination on critical surfaces of a space telescope leading to optical obscuration due to light scattering and hence degrading performance is another unwanted consequence.[12]

To develop effective strategies to control either desirable or undesirable deposition of particles, a sound understanding of the underlying particle transport mechanisms and the associated physical factors influencing the processes is required to gain insights into particle deposition behaviors. A significant body of scientific research has been devoted to studying the dynamic behavior of particles under well-defined configurations and air flow conditions—examples include aerosol-laden air flowing through fibrous filters,[13,14] particle deposition from turbulent channel flow,[15,16] and particle deposition from laminar, vertical flow onto a circular plate.[2,17–19] In contrast, not many published studies consider particle deposition onto surfaces in a three-dimensional confined space, probably due, in part, to the complexity of airflow patterns associated with enclosures of various geometrical shapes.

The goal of this report is to provide a state-of-the-art literature review concerning particle deposition onto surfaces within an enclosed volume. The knowledge gleaned from the available scientific publications presented here can be applied to an enclosure scale as small as a spacecraft payload cavity, or as large as a clean room in a manufacturing/processing facility. The surfaces of interest for particles to deposit on could be walls, the floor, the ceiling, or any contamination-sensitive surfaces within an enclosed volume relevant to various engineering applications.

The report begins with the characterization of airflow adjacent to a surface and how it relates to the core region of an enclosure. Particle deposition flux, a parameter used to evaluate the rate of deposition onto surfaces, is briefly introduced as the concept will be mentioned throughout the chapter. Next, the fundamental physical processes governing the transport of particles are discussed, and the definition of the parameters commonly reported in the literature for characterizing deposition are introduced, along with the available experimental techniques for their measurement. The dependence of particle deposition rate on particle size, airflow, and surface characteristics are examined from the existing published experimental investigations relevant to enclosures. Lastly, modeling developments for predicting the rate of particle deposition and associated experimental validations are presented.

2. Background

Knowledge of particle transport and deposition within an enclosed volume has been applied in numerous practical scenarios. In the beginning of this section, special attention is given to the relevance of particle deposition to contamination control in the context of space applications.

Since aerosol particles are transported to the vicinity of surfaces by air currents, understanding the nature of air flow and its near-surface characteristics is the first step to gain insights into the processes of particle deposition onto surfaces. In addition, a quantitative approach using the concept of *flux* and the underlying physical mechanisms that govern particle deposition are briefly described.

2.1 Relevance to Contamination Control in Space Applications

In space applications, the concern of particle deposition on contamination-sensitive surfaces arises from the undesirable effects of surface obscuration. For one thing, the presence of particles on optical reflective surfaces, e.g., mirrors and focal planes, interferes with the proper transmission of light to the next optical components, hence reducing the signal strength. Particles residing on an absorptive surface, such as baffles inside a telescope assembly, causes light scattering ,which, in turn, overwhelms the signal and ultimately may even damage other optical components. The presence particles on thermal control surfaces causes alterations of solar absorbance and/or emissivity, which leads to an altered equilibrium temperature, and may further deteriorate the thermal control function.

In light of the adverse effects due to particulate contamination, the aim of contamination control is to prevent performance degradation by minimizing the deposition of particles on critical and sensitive surfaces of spacecraft components. Meeting this objective is particularly important for high-profile remote sensing spacecraft, such as the Hubble Space Telescope. As a consequence, tremendous efforts and resources are dedicated to contamination control during various phases of spacecraft processing: design, manufacturing, assembly, testing, integration, storage, shipping, launch site ground activities, and in-flight operations.

The development of effective mitigation strategies to minimize particle contamination requires knowledge of particle transport and deposition as well as the associated physical factors affecting the processes. Spacecraft surface contamination as a result of particle fallout may take place at any level of engineering practice, for instance, component fabrication in a *cleanroom*, system assembly and testing within a *payload cavity*, and spacecraft integration inside *payload fairing*. Note that the terms in italics refer to the corresponding enclosed volumes under the example scenario considered; thus, one can see that the study of particle deposition onto surfaces in enclosures is of strong relevance to a variety of circumstances in space applications. The insights from studying the physical processes that influence the rate of particle deposition within an enclosure are expected to provide a strong scientific foundation to benefit various aspects of aerospace contamination control needs.

2.2 Nature of Air Flow and its Near-Surface Characteristics

Inside an enclosed volume, air is mixed through two mechanisms: natural convection and turbulent mixing (forced convection). Natural convection is driven by temperature gradients, i.e., temperature difference (ΔT) across the space inside the enclosure, induced by heat transfer at surfaces. Turbulent mixing or forced convection, on the other hand, is associated with external energy input into a system, such as fan mixing or fluid flushing. In an enclosure without the mechanism of forced convection, natural convection becomes the only cause for fluid mixing. Small temperature variations within the enclosure may induce convective currents, which, in turn, cause aerosol concentration to become mixed throughout the volume. It is estimated that the convective flow velocity can reach approximately 1 cm/s in a 1-m-high chamber when the floor or wall surfaces are warmer than the air by 0.01°C.[20] Study also has shown that a ΔT of 0.1°C can induce homogeneous mixing for particles up to 15 μm in diameter.[21] On the other hand, buoyancy can also impede mixing. For instance, a warm ceiling and cool floor will promote stratification of air masses within an enclosure. Some empirical evidence about near-surface airflows in rooms can be found in reference [22]

One widely accepted approach to model air flow in enclosures is to assume that the air in the core region is homogeneously and isotropically turbulent, behaving like an ideal nonviscous fluid. Adjacent to the interior surface, the air is assumed to behave as a viscous fluid within a thin layer, which is also known as the boundary layer. Inside the *momentum* boundary layer, the fluid velocity drops sharply to zero at the surface from its mainstream peak value. The thickness of the momentum boundary layer depends on the momentum diffusivity of the fluid. For instance, the typical thickness is about 1 to 2 cm for room air motion,[6] given air kinematic viscosity of 0.15 $cm^2\ s^{-1}$ at 293K and 1 atm.

The boundary layer concept can also be used to capture the near-surface characteristics in terms of thermal and contaminant concentration profiles. For air, the thickness of the thermal boundary layer is comparable to that of the momentum boundary layer because the thermal diffusivity (~0.2 $cm^2\ s^{-1}$ for air) is of the same order of magnitude as the momentum diffusivity. For gaseous contaminants with molecular weights close to those of N_2 and O_2, the thickness of the *concentration* boundary layer would be similar to that of the momentum and thermal boundary layer because the molecular diffusivities are comparable to momentum and thermal diffusivities. Airborne particles, however, have small diffusivities (or diffusion coefficients) compared to molecular contaminants, which leads to much thinner* particle concentration boundary layers than the momentum and thermal boundary layers. Okuyama et al.[23] estimated, from their experiments in a 2.6-L non-stirred cylindrical tank, the particle concentration boundary layer thickness to be approximately 0.3 cm when the particle diffusivity is $10^{-3}\ cm^2\ s^{-1}$. Considerable information about particle concentration boundary layer thickness can be found in references [24] and [25].

In addition to aerosol diffusivities, the nature and the intensity of the near-surface air flow also play a role in determining the thickness of the concentration boundary layer. Scale analysis[26] that is used to approximate particle boundary layer thickness adjacent to surfaces indicates that, given the same diffusivity, the boundary layers are thinner when the fluid outside them is fast moving, and thicker when the fluid moves slowly.

---

* As will be shown later in Subsection 6.3.2, the implication of a thinner concentration boundary layer is that small-scale surface roughness can play a significant role in affecting particle transport across the boundary layer, but have negligible effects on momentum and heat transfer.

In general, the air within an enclosure of arbitrary shape can be visualized to consist of two parts: a core zone where the air is well mixed, and a thin quiescent boundary layer adjacent to the inside surface of the enclosure where little air motion exists in the direction perpendicular to the surface (see Figure 1). In the core zone the particle concentration is often assumed to be spatially uniform due to well-mixed air flows, and large-scale turbulent (or eddy) diffusion is responsible for bringing aerosols to the vicinity of the surface for subsequent deposition.* Upon arrival at the boundary layer, aerosols may migrate through the thin layer to the surface by mechanisms such as Brownian/turbulent diffusion, gravitational settling, thermophoresis, inertial drift, and electrostatic attraction. These transport processes, as will be discussed in Section 3, commonly control the rate of particle deposition onto surfaces in enclosures.

In summary, the boundary layer concept used to characterize aerosol transport processes from mainstream fluid onto surfaces has been applied with great success in a large variety of air flow scenarios, such as external flows around cylinders or spheres, laminar and turbulent pipe flows, and enclosures with quiescent or turbulent flows. Theoretical developments based on this boundary layer concept to evaluate the extent of particle deposition within an enclosed volume along with the associated experimental validations will be discussed in more details in Subsection 7.1.

2.3 Evaluating Particle Deposition: Deposition Flux

The rate of particle transport onto a surface is commonly quantified in terms of a *deposition flux*, with the dimensions of mass (or number) per unit time per unit area. In the event that transport through the boundary layer is dominated by the combined effects of turbulent and Brownian diffusion, the flux of particles onto a smooth, isothermal, and electrically neutral vertical surface can be characterized by the following one-dimensional steady-state continuity equation.

$$\text{Flux} = -\left(\varepsilon_p + D\right)\frac{dC}{dy}, \tag{1}$$

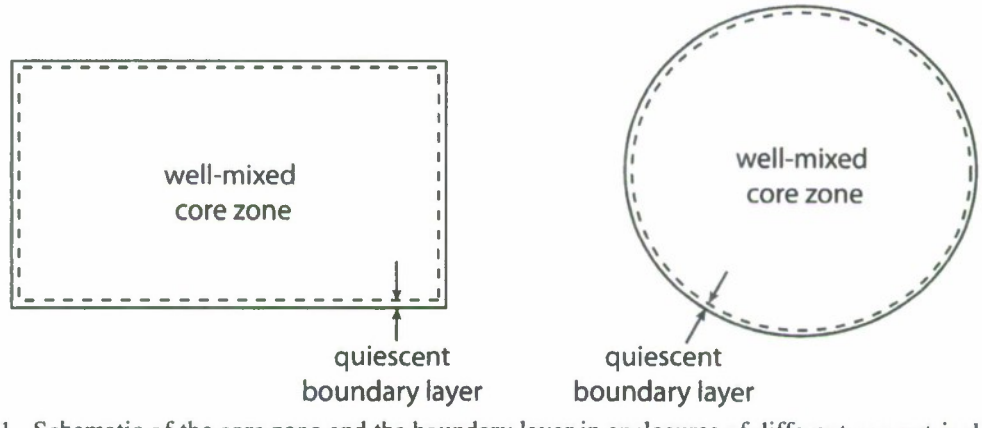

Figure 1. Schematic of the core zone and the boundary layer in enclosures of different geometrical shapes.

* Also known as "homogeneous turbulence model," and its theoretical representations will be addressed in Subsection 7.1.

where ε_p and D are the turbulent (or eddy) and Brownian diffusivities for aerosols, respectively; C is the aerosol concentration in air; and y is the distance from the surface.

Equation (1) can be viewed as a modified form of *Fick's first law of diffusion*, which describes the linear relationship between the flux of aerosols and the concentration gradient dC/dy, with the term $(\varepsilon_p + D)$ being the proportionality constant. Physically, this suggests that the net transport of particles, due to diffusion only, always takes place from regions of high to low particle concentration.

Equation (1) has long been used to evaluate particle deposition flux. Since the air flow outside the boundary layer is assumed to be homogeneously mixed, a particle concentration gradient only exists within the boundary layer. Other assumptions for this theoretical representation include: (1) particles are completely retained once they collide onto the surface, i.e., the surface acts as a perfect sink for particle deposition; and (2) no mechanisms of coagulation, condensation, and evaporation are involved during the transport process (i.e., there are no sources or sinks for particles within the boundary layer); thus, the particle flux is constant throughout the particle concentration boundary layer.

In the presence of particle transport mechanisms other than diffusion, the particle flux can be evaluated by adding terms to account for external force fields acting on the particles, and that gives

$$\text{Flux} = -(\varepsilon + D)\frac{dC}{dy} - v_e C\,, \tag{2}$$

where v_e is the particle steady-state drift velocity under the action of external body forces counteracted by fluid drag. The external force fields of most interest in particle deposition processes include gravitational, electrical, and thermal (generated by a temperature gradient in the fluid), as will be presented in the next section.

3. Mechanisms of Particle Transport

Airborne particles are transported onto surfaces through a variety of physical processes, so-called deposition mechanisms. The fundamental physics behind particle transport or movement from one point to another is universal, regardless the configurations of the system, for instance, dust accumulation in ventilation ducts, gas cleaning by particle collection on fibrous filters, and scavenging of particulate matter from the atmosphere. Below, the underlying physical processes governing particle motion in air are addressed.

3.1 Brownian Diffusion

Brownian diffusion is the characteristic random wiggling motion of small airborne particles in still air, resulting from constant bombardment by surrounding gas molecules. Such irregular motions of pollen grains in water were first observed by the botanist Robert Brown in 1827, and later similar phenomena were found for small smoke particles in air. In the early twentieth century, the relationships characterizing Brownian diffusion based on kinetic theory of gases were first derived by Einstein in the early 1900s, and later verified through experiments.[20]

The Brownian diffusivity, D (or diffusion coefficient), which relates the gas properties and the particles through fluid drag, can be evaluated by the Stokes-Einstein expression.[27,28]

$$D = \frac{kTC_c}{3\pi\mu d_p}, \tag{3}$$

where k is Boltzmann's constant (1.38×10^{-23} J K^{-1}), T is the absolute temperature in K, μ is dynamic viscosity of air, d_p is particle diameter, and C_c is a slip correction factor for small particles (see Subsection 3.3 for details). The value of D depends on the particle size and fluid properties. For instance, the diffusivity of a 0.01-μm aerosol particle is 20,000 times higher than that of a 10 μm aerosol particle. The larger the value of D, the more rapid the mass transfer process to drive particles moving from regions of high to low concentration. Brownian diffusion is the dominant particle deposition mechanism for small particles (<0.1 μm) over short distances.

3.2 Turbulent Diffusion

For particle transport on greater physical scales (i.e., larger distance), turbulent diffusion is far more effective than the thermal-based Brownian diffusion. Mass transfer of particles from one point to another by turbulent (or eddy/convective) diffusion is analogous to momentum transfer by fluctuating velocity components in turbulent flows. Unlike momentum transfer inside the thin stagnant layer of air adjacent to a surface where viscous forces are dominant and turbulence fluctuations are negligible, mass transfer of particles is attributed to the combination of turbulent and Brownian diffusion. A

general expression for the particle flux to the surface due to both turbulent and Brownian diffusion was described in Eq. (1), with the derivations shown in reference [27].

Intuitively, the particle turbulent diffusivity, ε_p, inside the boundary layer is expected to vary with distance from the surface, y, owing to the physical constraints imposed by the surface. In fact, it is extremely difficult to determine the value of ε_p explicitly because it is strongly associated with the degree of turbulence with respect to the air flow structure in the system, as well as with the size of particles (e.g., heavy particles cannot faithfully follow the fluid eddies). Hinze[29] has shown that over a sufficiently long time scale, the particle turbulent diffusivity equals the fluid turbulent viscosity by solving the equation of motion for a particle in a homogeneous turbulent flow field. A similar argument made by Fuchs[20] is that the motion of larger particles is more persistent due to their larger mass, which, in turn, contributes to the nearly identical average distance traveled by large and small particles over a long time limit. Additionally, numerical simulation of turbulent diffusion of particles also indicated that particle and fluid turbulent diffusion are comparable for particles smaller than approximately 170 μm.[30] Therefore, it is a fair statement that the turbulent diffusivity for particles can be reasonably approximated as the same order of magnitude as that of gas fluid ($\sim 10^{-1}$ cm^2 s^{-1}), which is far greater than the particle Brownian diffusivities. In other words, particles tend to migrate closer to the surface by turbulent diffusion before Brownian diffusion becomes important.

In essence, particle turbulent diffusivity gradually diminishes in the particle concentration boundary layer to zero at the surface. Throughout the core of an enclosure, turbulent diffusivities can vary over large ranges in accordance with the intensity of air motion.

3.3 Drag Force

Fluid drag on a particle is the resistance force exerted by the surrounding fluid when there is relative motion between the particle and the fluid. In other words, the drag force is always present as long as the particle is not travelling in a vacuum. The net effect of the drag force is to reduce the acceleration of particles.

The drag force, F_D, on a spherical particle can be characterized by Stokes's law:

$$F_D = 3\pi\mu V d_p, \tag{4}$$

where V is the particle speed relative to the local fluid speed. Stokes's law is derived from the solution of the Navier-Stokes equations, assuming* that inertial forces are negligible compared to viscous forces and that the fluid speed at the particle's surface is the same as the particle's. Owing to the low velocities and small particle sizes involved, most aerosol motions occur at low particle Reynolds numbers ($Re_p << 1$), where $Re_p = d_p V/\nu$, expressing the ratio of inertial to viscous forces on particles.

* Other assumptions include: incompressible fluid, no walls or other particles nearby, constant motion, zero fluid velocity at the particle's surface, and rigid spherical particles. These assumptions work well in most cases for aerosols. See Hinds[28] for more detailed discussions.

Table 1 shows the calculated Re_p for spherical particles of different sizes falling at their steady-state settling velocity in air due to gravity. By looking at Re_p, Stokes's law clearly holds true for particles smaller than 20 μm. For aerosols that are relatively large and move through a fluid rapidly, the inertial forces become dominant compared to viscous forces; thus, the drag force exerted to the particle is calculated as

$$F_D = \frac{\pi}{4} d_p^2 \left(\frac{1}{2} \rho V^2 \right) C_d , \tag{5}$$

where C_d is the drag coefficient, given by reference [31]

$$C_d = \begin{cases} \dfrac{24}{Re} & Re << 1 \text{ (Stokes's law)} \\ \dfrac{24}{Re}\left[1 + \dfrac{3}{16} Re + \dfrac{9}{160} Re^2 \ln(2\,Re)\right] & 0.1 < Re < 2 \\ \dfrac{24}{Re}\left(1 + 0.15\,Re^{0.687}\right) & 2 < Re < 500 \\ 0.44 & 500 < Re < 2 \times 10^5 \end{cases} \tag{6}$$

When the size of an aerosol particle approaches the mean free path of gas molecules (0.066 μm for air at 1 atm and 20°C), the assumption of zero relative fluid velocity right at the particle surface fails, which could lead to significant errors. In this case, the actual drag force is smaller than predicted by Stokes's law. A correction parameter, the Cunningham correction factor, C_c, is introduced to correct for this "slip" phenomenon for small particles, and the corrected Stokes's law becomes

$$F_D = \frac{3\pi\mu V d_p}{C_c} , \tag{7}$$

Table 1. Particle Reynolds Numbers (Re_p) Calculated for Particles of Different Diameters Falling at Their Terminal Settling Velocities in Air at 20°C, Pressure = 1 atm, and Gravitational Acceleration = 980 cm s^{-2}

Particle diameter, μm	Re_p
0.1	5.8×10^{-9}
1	2.3×10^{-6}
10	2.0×10^{-3}
20	1.6×10^{-2}
50	0.25
100	2
300	20

$$C_c = 1 + \frac{\lambda}{d_p}\left[2.514 + 0.800\exp\left(-0.55\frac{d_p}{\lambda}\right)\right], \quad (8)$$

where λ is the mean free path of gas molecules. The empirical formula of Eq. (8) allows the extension of Stokes's law to aerosol size below 0.01 μm. It is important to include the slip correction factor for particles whose diameter is smaller than about 10 times the mean free path of gas molecules.

3.4 Gravitational Settling

Gravity imposes an overall downward drift on particles, which contributes an enhanced deposition flux on surfaces with an upward component to their orientation. The gravity force exerted on a particle is

$$F_g = \frac{\pi}{6} d_p^3 (\rho_p - \rho_a) g \ , \quad (9)$$

where g is the acceleration due to gravity (9.81 m s^{-2} at the Earth's surface), and ρ_p and ρ_a are particle and air densities, respectively. The buoyancy effect usually can be neglected because ρ_a is commonly much smaller than ρ_p.

The terminal settling velocity of a particle, v_{ts}, is established when the gravity force is balanced by the fluid drag force, and it is expressed as[27,28]

$$v_{ts} = \frac{C_c \rho_p d_p^2 g}{18\mu} . \quad (10)$$

As suggested in Eq. (10), the particle terminal settling velocity increases rapidly with particle size since it is proportional to the square of particle diameter for supermicron particles (where $C_c = 1$). Assuming unit particle density, for instance, the settling velocities for 1 μm and 10 μm particles are 3.50×10^{-3} cm/s and 3.05×10^{-1} cm/s, respectively.

3.5 Thermophoresis

In the presence of a temperature gradient, aerosol particles are driven from the high to low temperature regions; this transport process is known as thermophoresis. The phenomenon was first reported in the 19th century,[32] and its quantitative descriptions were published by Watson in 1936[33] and Zernik in 1957.[34]

Thermophoretic force arises from asymmetrical interactions of an aerosol with the surrounding gas molecules in a temperature gradient, where gas molecules on the warm side bombard the particle with

higher average momentum than those on the cooler side. Acting in the direction of decreasing temperature, thermophoretic force can be expressed as[35]

$$F_{th} = -\frac{3\pi\mu^2 d_p H}{\rho_a T}\frac{dT}{dy}, \tag{11}$$

where dT/dy is the temperature gradient, and H is the thermophoretic force coefficient, given by

$$H = \left(\frac{2.34}{1+6.84\lambda/d_p}\right)\left(\frac{k_a/k_p + 4.36\lambda/d_p}{1+2k_a/k_p + 8.72\lambda/d_p}\right), \tag{12}$$

where k_a and k_p are the thermal conductivities of air and the particle material, respectively.

When the thermophoretic force on a particle is balanced with fluid drag, the thermophoretic velocity is obtained as

$$v_{th} = -\frac{C_c \nu H}{T}\frac{dT}{dy}. \tag{13}$$

Contrary to gravitational settling and Brownian diffusion, which are strong functions of particle size, the thermophoretic velocity is nearly independent of particle size for particles smaller than 1 μm. This occurs because both the thermophoretic force and fluid viscous drag have approximately the same dependence on particle diameter. For larger particles, the thermophoretic velocity decreases with increasing particle size in a manner that depends on the relative thermal conductivities of the particle and of air.

3.6 Electrostatic Force

A charged particle migrates in an electrical field due to the Coulomb force F_C, which is given by

$$F_C = qE = n_e eE, \tag{14}$$

where q is the charge on the particle, E is the electric field strength, n_e is the number of electrons of deviation from the electrically neutral state (including sign), and e is the charge of a single electron (-1.6×10^{-19} C).

In the absence of an electrical field, charged aerosols will migrate towards or away from a conducting surface, owing to the image force, dielectric force, and dipole-dipole force, although these forces are much weaker than the Coulomb force. The overall electrostatic force on a charged particle can be predicted by[36]

$$F_E = qE - \frac{q^2}{16\pi\varepsilon_o y^2} + \frac{qEd_p^3}{16y^3} - \frac{3\pi\varepsilon_o d_p^6 E^2}{128y^4}, \quad (15)$$

where ε_o is the permittivity of air (8.86×10^{-12} $C^2 N^{-1} m^{-2}$), and y is the normal distance from a surface. The terms on the right-hand side of Eq. (15) account for the Coulomb force, image force, dielectric force, and dipole-dipole force, respectively. When an electrical field is present, the Coulomb force dominates, and both the dielectric and dipole-dipole forces are negligible. In the absence of an electric field, however, the only electrostatic force responsible for particle motion is the image force, as suggested in Eq. (15). The image force, which only occurs near a conducting surface, is always directed toward a surface and may dominate over Brownian diffusion and turbulent dispersion when extremely close to a surface. On electrically insulating materials, charges may accumulate on the surfaces, giving rise to electric fields, which, in turn, affect deposition of charged particles.

It should be noted that aerosol particles acquire or lose their charges through random collisions with airborne ions, which are formed by ubiquitous ionizing radiation. In the absence of an electrical field, the processes of aerosol acquiring and losing charges will eventually lead to an equilibrium charge state called Boltzmann equilibrium. The maximum number of charges carried by a particle depends on the size of the particles. Table 2 shows the distribution of charges carried by aerosols at Boltzmann equilibrium. Take 10-μm particles, for example. At equilibrium, only 4.3% of the particles are electrically neutral, and nearly 70% of the aerosol particles carry more than 3 charges on a single particle (either positive or negative).

For highly charged aerosols in an electrical field, the drift velocity resulting from electrostatic forces on particles can be thousands of times greater than that from the gravitational force.

Table 2. Distribution of Charge on Aerosols at Boltzmann Equilibrium (Reproduced with permission from Hinds, 1999, John Wiley & Sons, Inc.[28])

Particle Diameter (μm)	Percentage of Particles Carrying the Indicated Number of Charges								
	< -3	-3	-2	-1	0	+1	+2	+3	> +3
0.01				0.3	99.3	0.3			
0.02				5.2	89.6	5.2			
0.05			0.6	19.3	60.2	19.3	0.6		
0.1		0.3	4.4	24.1	42.6	24.1	4.4	0.3	
0.2	0.3	2.3	9.6	22.6	30.1	22.6	9.6	2.3	0.3
0.5	4.6	6.8	12.1	17.0	19.0	17.0	12.1	6.8	4.6
1.0	11.8	8.1	10.7	12.7	13.5	12.7	10.7	8.1	11.8
2.0	20.1	7.4	8.5	9.3	9.5	9.3	8.5	7.4	20.1
5.0	29.8	5.4	5.8	6.0	6.0	6.0	5.8	5.4	29.8
10.0	35.4	4.0	4.2	4.2	4.3	4.2	4.2	4.0	35.4

3.7 Turbophoresis

Turbophoresis is a phenomenon in which the net migration of particles occurs from regions of high to low turbulence intensity, i.e., toward surfaces where the turbulent velocity fluctuations decrease to zero. Physically, particles in regions of high turbulence intensity acquire sufficient fluctuating velocity components, which enable them to drift to regions where the turbulence intensity is too low to send them back with sufficient momentum for the return journey.

Based on the analogy between Brownian motion and turbulent diffusion, as well as energy transfer from the fluid to the particle, the mathematical expression for turbophoretic velocity V_t was first proposed by Caporaloni *et al.*[37] as

$$V_t = -\frac{C_c \rho_p {d_p}^2}{18\mu} \frac{d\left(\overline{v_y'}\right)^2}{dy}, \tag{16}$$

where $\overline{v_y'}$ is the fluctuating particle velocity normal to the surface. Reeks[38] deduced the term for the turbophoretic effect and arrived at the same expression in a much more rigorous approach (a special closure of Liouville particle equation of motion).

Distinctly different from turbulent diffusion, turbophoresis is attributed to the interaction between particle inertia and the inhomogeneous turbulent flow field, and the mass transfer takes place against the gradient in turbulence intensity, even in the absence of a concentration gradient. The effect of turbophoresis is only significant for particles with sufficiently high inertia, and is typically only relevant in the vicinity of a surface where the gradient in turbulence intensity is high.

For near-surface inertial particles under highly turbulent flow scenarios, particle transport models accounting for turbophoresis have shown good agreements with experimental measurements.[39–41]

4. Parameters for Particle Deposition Characterization

To characterize the rate of particle deposition in an enclosure, deposition velocity (v_d) and particle deposition rate (β) are the two parameters commonly reported in the literature. Here, their definitions, derivations, and physical implications, as well as the distinctions between β and v_d are discussed.

4.1 Deposition Velocity, v_d

Particle deposition, a mass transfer process of airborne particles onto surfaces, occurs by a first-order, irreversible mechanism. Being "first-order" suggests that particle deposition flux is linearly proportional to the airborne concentration, and being "irreversible" means that particles simply adhere once they collide with surfaces.

The aerosol deposition rate can be parameterized in terms of a mass transfer coefficient, known as the deposition velocity, v_d. It is considered as the proportionality constant between the net aerosol flux J and the free-stream airborne concentration, C_∞.

$$v_d = \frac{J}{C_\infty} [=] \frac{\text{mass / area} \cdot \text{time}}{\text{mass / volume}} [=] \frac{\text{length}}{\text{time}}. \tag{17}$$

The aerosol concentration, C_∞, is determined at a position sufficiently far away from the surface, i.e., core zone in an enclosure, so that the concentration should not vary greatly with positions.

With dimensions of length per time, deposition velocity appears to represent an effective velocity, which incorporates all of the complexities of the particle deposition process. In other words, deposition velocity, as an aggregated term, comprises every aspect of particle deposition processes, including (1) aerodynamic transport of particles by turbulent diffusion from the well-mixed core region to the thin boundary layer of air adjacent to the surface; and (2) mass transfer of particles across the boundary layer, and subsequent uptake by the surface through a variety of particle deposition mechanisms.

The magnitude of the deposition velocity depends on factors that govern particle transport: particle size, the near-surface air turbulence, surface characteristics including orientation and texture (smooth vs. rough), air-surface temperature difference, and the presence of an electrical field near the surface. A literature review of the existing experimental findings concerning the influence of these factors on particle deposition is presented in Section 6.

4.2 Particle Deposition Rate, β

Another common parameter used to quantitatively characterize the particle deposition rate β in an enclosure is defined as:[20]

$$\frac{dC(d_p,t)}{dt} = -\beta C, \tag{18}$$

where $C(d_p,t)$ is the aerosol number or mass concentration as a function of time, t, in the core region of the enclosure, and β is the particle deposition rate with the unit of time^{-1} (e.g., s^{-1}). Particle deposition rate is also commonly referred to as the *aerosol removal rate* or *wall loss rate* because the deposition process removes particles from the gas phase onto the available wall surfaces.

Equation (18) is written in the form of mass balance of particles suspended in air within an enclosure, with the following conditions: (1) no or negligible sources for particle generation (such as particle influx in the incoming air flow and nucleation); (2) no particle size change due to coagulation,* condensation, and evaporation; and (3) deposition onto surfaces is the only particle loss mechanism. Note that the particle deposition rate is expected to be a function of particle size, as is the case for particle deposition velocity. Also note that Eq. (18) only accounts for particle loss attributable to deposition. In an enclosure, there are typically other processes occurring in parallel, such as air exchange, that influence the particle concentration and should be taken into account.[6]

Experimentally, the aerosol concentration decays with time as expressed by Eq. (18) after initial mixing of aerosols in an air-tight enclosure. Mathematically, the rearrangement of Eq. (18) gives

$$C_t = C_o e^{-\beta t}, \tag{19}$$

where C_o is the initial aerosol concentration in the enclosure, C_t is the aerosol concentration at time t. When the air is well-mixed, plotting lnC as a function of time gives rise to a linear plot, with the negative of the slope yielding the particle deposition rate, β. Figure 2 represents an example of particle concentration decay as a function of time and the associated deposition rate. Similar to particle deposition velocity v_d, β incorporates all the deposition processes that remove aerosols from being suspended in the enclosure.

4.3 Comparison of v_d and β

The major distinction between v_d and β is that v_d depends on surface orientations with respect to gravity (a "local" parameter), while β represents an average term over all available surfaces for deposition within an entire enclosure (a "global" parameter). For instance, in the context of a

---

* Particle coagulation, which contributes to aerosol size distribution change, occurs when the aerosol concentration is sufficiently high. When that occurs, coagulation may be an important mechanism to incorporate in Eq. (18), as seen in Okuyama *et al.*[23]

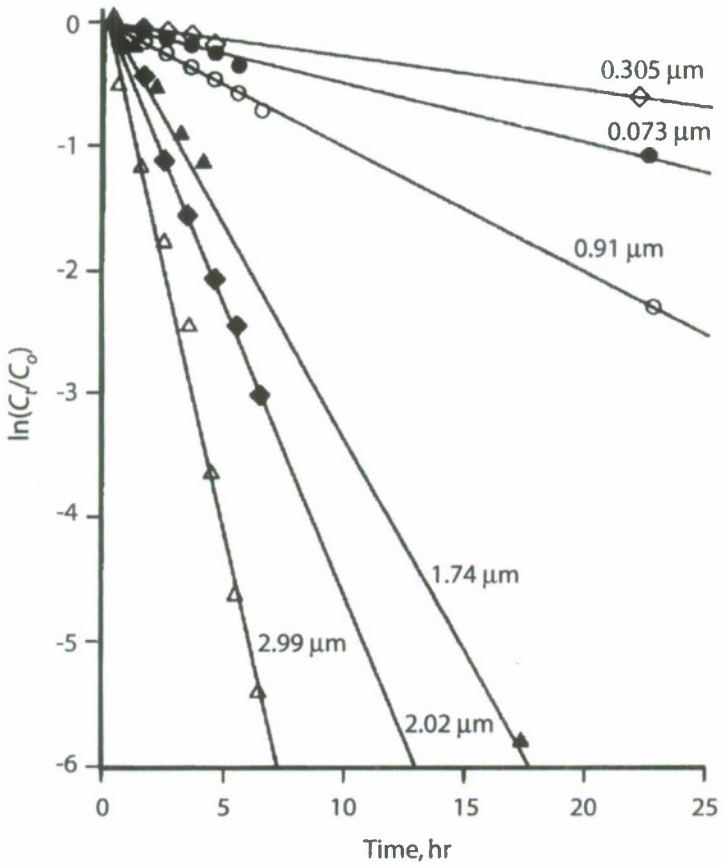

Figure 2. An illustrative example of aerosol concentration decay measurements of various particle diameters as a function of time in a 165-L cylindrical chamber (reprinted with permission from Chen *et al.*[42]). The particle deposition rates, obtained from the values of the slope, were 0.058, 0.14, 0.088, 0.28, 0.44, 0.71 h^{-1} for particle diameters of 0.305, 0.073, 0.91, 1.74, 2.02, and 2.99 µm, respectively.

rectangular enclosure, the magnitude of v_d for supermicron particles varies strongly with surface orientation, i.e., $v_{d,floor} > v_{d,wall} > v_{d,ceiling}$, owing to the dominant contribution of gravitational settling over diffusion and other mechanisms.

The value of β can be related to the values of v_d for all enclosure surfaces. By material balance, the deposition rate, β, is the surface-area-averaged v_d multiplied by the surface-to-volume ratio (S/V) of the enclosure:

$$\frac{dC}{dt} = -\frac{C}{V}\int v_d(s)ds = -C\frac{S}{V}\overline{v_d} = -\beta C, \qquad (20)$$

where $v_d(s)$ is the particle deposition velocity onto the surface s. The integration is to be carried out over all the enclosure interior surfaces with the total surface area S, and $\overline{v_d}$ is the area-weighted mean

deposition velocity. It can be clearly seen that β, unlike v_d, eliminates the explicit spatial dependence of particle deposition.

5. Methods for Measurement of Particle Deposition

Owing to its importance for numerous engineering systems, the processes of particle deposition on surfaces have been widely studied experimentally. Here, the general approach for measuring β and v_d with respect to an enclosed system is presented with the aim of helping to gain insights into the experimental findings that will be presented in Sections 6 and 7, respectively.

5.1 Measuring Particle Deposition Rate, β

Experimentally, the particle deposition rate β as a function of particle diameter is inferred from aerosol concentration decay over time, following Eq. (18) and as shown in Figure 2. To do so, monodisperse aerosols are usually generated in elevated concentrations so that sufficient time is available to take multiple data points on aerosol concentrations during the course of deposition experiments. When the test aerosols are polydisperse, the aerosol measuring instruments will need to have the particle size-resolved capability in order to determine the concentration decay rate as a function of particle diameter. The operation principles for some common particle sizing instruments, e.g., optical particle counter, time-of-flight aerosol spectrometer, electrical aerosol mobility analyzer, as well as aerosol generation methods, can be found in references [28,43,44].

Note that the degree of air turbulence plays an important role in influencing the rate of particle deposition. Therefore, the stirring of air within the experimental chamber, by either impeller mixing or flushing, should be controlled consistently throughout the experiment.

The scheme of determining particle deposition rate by monitoring airborne particle concentration decay over time does not involve direct measurements of deposited particles on surfaces, thus the measured deposition rate is "inferred." This type of experiment is relatively simple to carry out, and data analysis is straightforward. However, the drawback of this indirect approach is the inability to differentiate the contribution of particle deposition on surfaces with respect to orientations and locations.

5.2 Measuring Particle Deposition Velocity, v_d

As suggested in Eq. (17), particle deposition velocity is determined by normalizing the deposition flux with the average aerosol concentration over the duration of particle deposition. Distinct from measuring the deposition rate constant, β, evaluating v_d requires a direct measurement of particle deposition, which involves the simultaneous determination of particle deposition flux and airborne particle concentration. In other words, the deposited particle mass will need to be recovered from the surface (or otherwise detected and quantified), and the aerosol concentration outside the boundary layer during the course of deposition will also need to be determined. For the typical experiment of this type, monodisperse aerosols need to be generated and injected into the experimental chamber to provide the size-specific deposition flux. To obtain the deposition velocity as a function of particle diameter, the same experimental procedures are repeated for other particle sizes of interest. The

advantage of this direct measurement, albeit time-consuming and labor-intensive, is that spatially resolved particle deposition can be determined. A key challenge of this approach, however, is the need to accurately determine trace amounts of particles deposited on surfaces. The earliest method was performed by microscopically counting the particles on a small area of a test surface.[45] Despite the recent rapid advancement of optical and digital imaging techniques, it remains a tedious task to perform the counting, considering that only a very small surface area is available per microscopic frame, which, in turn, limits the possibility of sampling larger surface areas.

To quantitatively determine deposited particle mass on surfaces, aerosols can be labeled to facilitate subsequent surface analysis. Two types of tracer aerosol detection techniques have been employed for such purposes: (1) fluorescence spectroscopy, and (2) neutron activation analysis (NAA) or proton-induced X-ray emission (PIXE). With respect to the former method, monodisperse aerosols are generated with fluorescent materials. After deposition, the fluorescent particles on the test surface are extracted with a solution of known volume. The resulting fluorescence intensity of the solution is proportional to the collected particle mass from the surface.[46–48] In order to accumulate sufficient fluorescent particle mass for analysis, the experimental deposition time, particularly for submicron particles, could easily exceed 100 h.[46]

Contrary to the chemistry-based fluorescence technique, NAA or PIXE relies on the physics of atoms in the aerosol materials. In NAA, the energy of the induced radioactivity through neutron bombardment is characteristic of a particular element, while PIXE involves the measurement of the characteristic X-ray emission via high-energy proton excitations of the elements in the sample. Methods using NAA and PIXE are semi-invasive; i.e., only the particle-bearing surface needs to be removed for the analysis from the test chamber, and removal of deposited particles from the particle-bearing surface is not required. To minimize interfering effects from various elements, rare earth elements such as dysprosium (^{164}Dy) and indium (^{115}In) can be incorporated into the aerosols for the purpose of subsequent NAA analysis.[49–51] Owing to the extremely high sensitivity, for instance, a ^{164}Dy mass of the order of 10^{-10} g can be easily detected; hence, the experimental deposition time can be significantly reduced (e.g., 15–20 min).[50] The drawback of this technique, however, is that specialized facilities, such as a nuclear reactor for neutron activation, is required.

6. Review of Experimental Studies

A significant body of experiments has been devoted to exploring particle deposition in enclosures since the late 1940s due to the relevance to material deterioration and the implications to human health risk, etc. Table A1 in the Appendix highlights a chronological summary of the laboratory investigations pertaining to particle deposition in an enclosed environment.

The processes of particle deposition onto surfaces are complex, multifaceted phenomena since they vary strongly depending on the characteristics of particles and airflow patterns, as well as surface properties. In brief, the processes of particle deposition consist of two mechanisms in series: (1) particle transport from the core region in the enclosure to the boundary layer adjacent to the surface, and (2) subsequent deposition onto the surface. Consequently, both properties of airflow and the surface play a crucial role in governing the rate of particle deposition in steps (1) and (2), respectively. The degree of airflow turbulence controls how rapidly particles migrate to the proximity of a surface, while the surface characteristics, such as orientations and roughness, determine how readily particles interact with the surface. As will be seen soon, particle size is the most important parameter governing the motions of particles in a gas phase associated with the transport properties.

Here, the important physical factors that influence particle deposition onto enclosure surfaces are summarized from the existing literature.

6.1 Particle Characteristics Affecting Particle Deposition

Particle size is key in the determination of particle deposition. The dimension of particles in the gas phase is commonly characterized in terms of aerodynamic diameter, which refers to an equivalent diameter of a unit density spherical particle with the same terminal settling velocity as the particle being measured.[27] Therefore, the concept of aerodynamic diameter has taken particle shape and density into account, and it has successfully captured the aerodynamic behavior of airborne particles in many systems of interest.* The notion of aerodynamic diameter has been commonly used in the aerosol literature, including this review.

Figure 3 illustrates the characteristic V-shaped curves of experimentally determined particle deposition rates as a function of particle diameter. The large variability of the data, which can be up to 2 orders of magnitude, reflects the fact that other factors, such as airflow turbulence and surface characteristics, also play a significant role in influencing the extent of particle deposition in enclosures. As mentioned earlier, when particles are not electrically charged, the rate of particle deposition is governed by gravitational settling and Brownian motion of particles, as well as the turbulent motion of the fluid in which particles are entrained. For particles smaller than 0.1 μm, Brownian and turbu-

* The behavior of nonspherical particles in shear flows might not be properly characterized using the concept of aerodynamic diameter owing to their complex rotational and translational motions not accounted for in spherical particles. Thus, the prediction and measurement of deposition using aerodynamic diameters for nonspherical particles under this scenario would be an average outcome contributing from their stochastic behaviors in the turbulent flow.

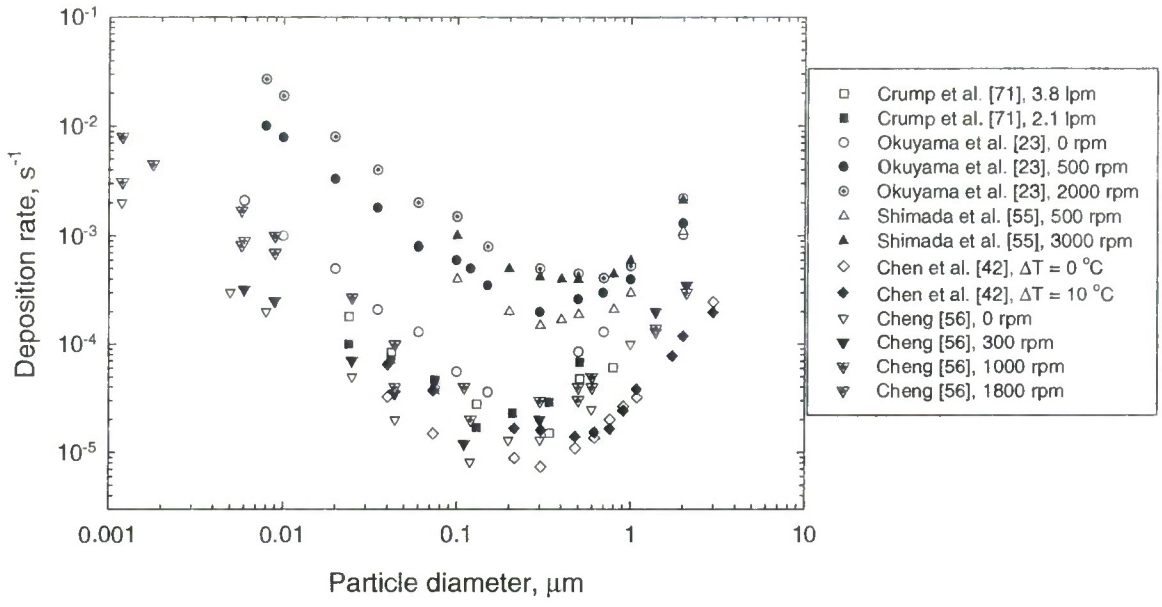

Figure 3. Comparison of experimentally obtained particle deposition rates as a function of particle diameter. The values of particle deposition rate β exhibit distinct minima for 0.1–1 μm particles, as indicated in the V-shaped curves.

lent diffusion control particle deposition. On the other hand, gravitational settling becomes dominant in removing particles from the gas phase with the increase of particle size, e.g., >1 μm. As a result, a minimum of particle deposition rate occurs for particles of 0.1–1 μm, which are generally referred to "accumulation mode" particles, when neither of the mechanism works effectively to cause particle deposition (Figure 3).

With respect to particle composition, experiments have shown that the material of particles makes no difference in the measured particle deposition rates.[23] Also, as seen in Table A1, various aerosol materials have been employed for particle deposition experiments, and the choice of aerosol compositions does not alter the outcome.

6.2 Airflow Characteristics Affecting Particle Deposition

Carried by large-scale eddy currents, airborne particles are brought from one point to another by turbulent diffusion. Eddy currents can be induced by natural convection (e.g., temperature gradient), and forced convection (e.g., mechanical stirring and fluid flushing).

6.2.1 Forced Convection

Early experimenters observed that increasingly turbulent air motion in an enclosed space was related to enhanced particle deposition onto surfaces, and the empirical parameters describing such phenomena were obtained as a function of the air stirring intensity.[52] Corner and Pendlebury[53] later explained these empirical observations based on the theoretical grounds, and concluded that air turbulence was one important factor that influenced the rate of particle deposition.

Subsequent experiments help to shed light on the dependence of particle deposition rates on the air turbulence level in the enclosures. Figure 4 represents four laboratory results of particle deposition rates with respect to different air mixing scenarios. It can be seen that enhanced particle deposition is attributed to increased air turbulence, which was produced by either fluid flushing (Nomura *et al.*[54]) or fan stirring (Okuyama *et al.*[23], Shimada *et al.*[55], and Cheng[56]). The enhancement of particle deposition onto enclosure surfaces results from more effective aerodynamic mass transfer at higher airflow turbulence, which brings aerosol particles more rapidly toward a surface.

In addition, as the turbulent fluctuation of air motion becomes significant, particle inertia may contribute to particle deposition, and inertial transport of particles through the boundary layer could be potentially enhanced by near-surface turbulent bursts.[41] Inertially induced turbulent deposition could be particularly important for large particles.

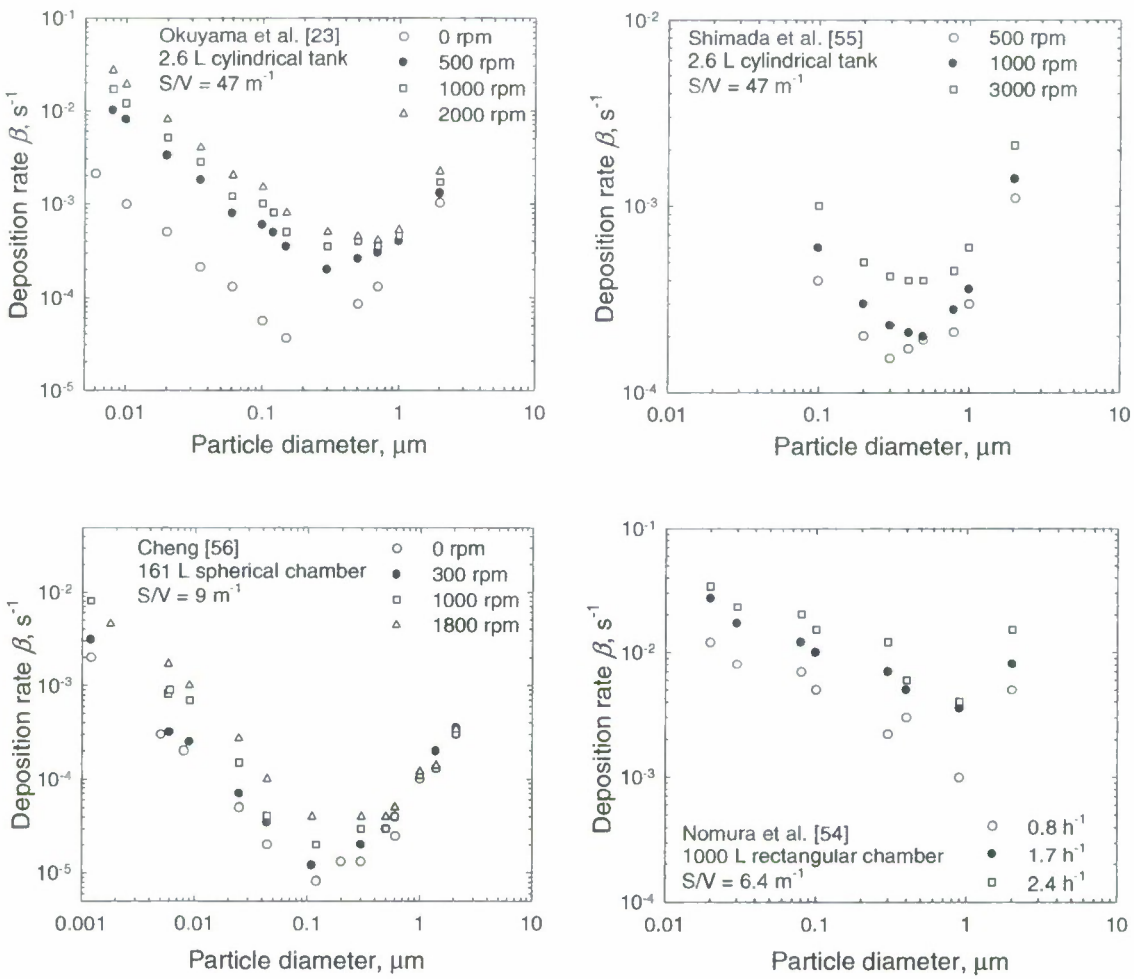

Figure 4. Dependence of experimentally measured particle deposition rates on the degree of airflow turbulence, as characterized by the fan stirring rate (in rpm) and the air-exchange rate (incoming airflow rate divided by the enclosure volume, with the unit of h^{-1}). The interior surface area-to-volume ratio, S/V, is indicated for each test chamber. Within the same experimental system, enhanced particle deposition is consistently observed at higher air turbulence levels.

6.2.2 Natural Convection

Natural convection arises from temperature differences among air parcels, or heat transfer at surfaces (i.e., surface-to-air temperature difference). In the absence of forced convection, natural convection becomes the only means of air mixing inside enclosed spaces. Cheng[56] conducted particle deposition experiments under isothermal and still air conditions with no apparent air movements detected* in the chamber, but still found the deposition data well described by the homogeneous turbulence model, assuming the core region was well-mixed (see Subsection 7.1 for more discussion).

Figure 5 shows a comparison of particle deposition rates as a function of particle size under natural convection conditions from different experiments.[23,42,56–58] First, notice that particle size remains the predominant parameter governing the deposition rates, as indicated by the distinct V-shaped curves. Secondly, the scatter of the data in these experiments may be attributed to (1) the S/V ratio, as higher surface area normalized by volume translates to more surfaces available for particles to deposit on, and (2) temperature gradient within the enclosure, as it dictates the extent of convective mixing. Chen *et al.*[42] and Cheng[56] specifically documented the temperature measurements inside their test chambers, ensuring that the experimental systems were either isothermal or otherwise reported. The temperature data from the other deposition measurements are either insufficient or unavailable to draw any useful information.

6.3 Surface Characteristics Affecting Particle Deposition

After airborne particles enter a boundary layer, they may be transported to the surface by means of a variety of deposition mechanisms, as described in Section 3. It remains a good approximation and has been demonstrated experimentally that adhesion of micrometer-sized (or smaller) particles is

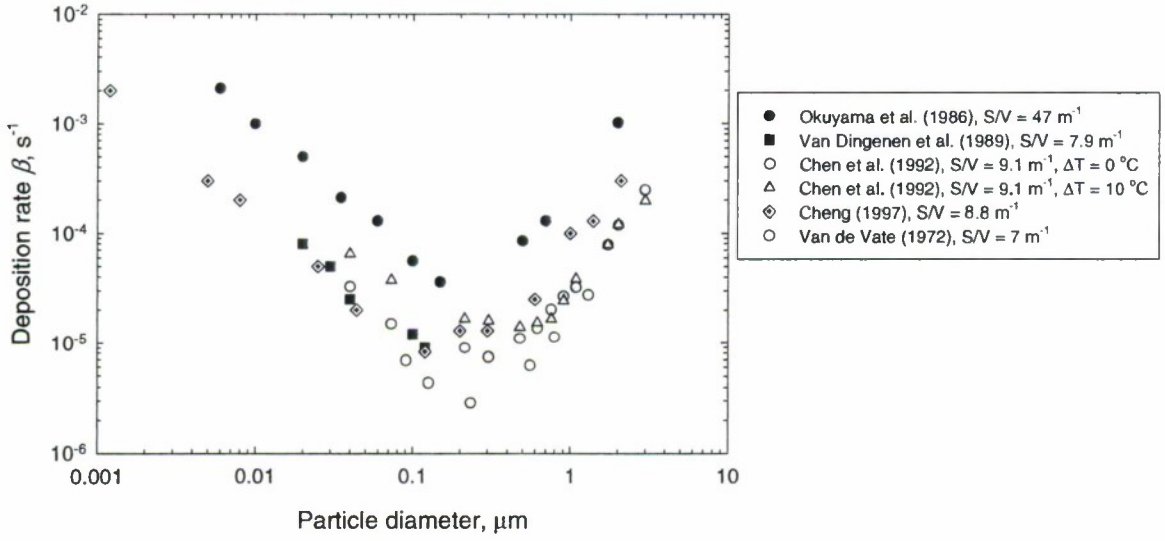

Figure 5. Comparison of experimentally measured particle deposition rates as a function of particle size under natural convection conditions. The interior surface area to volume ratio, S/V, is indicated for each experimental chamber. ΔT in Chen *et al.*[42] refers to the temperature difference between the top and bottom walls (e.g., $T_b - T_t = 10°C$) of the test chamber.

* The detection limit in these experiments was about 1 cm/s.

complete and irreversible once they come into contact with a surface.[59] The Van der Waals force is the predominant adhesion force between an aerosol particle and any surface (including another particle), although electrostatic and capillary forces may be important as well.[28]

Surface characteristics play a role influencing particle deposition as they often affect particle-surface interactions within the boundary layer. The dependence of particle deposition on surface characteristics has been explored experimentally by manipulating various factors such as surface orientations and roughness. Below, an overview is provided concerning experimental deposition studies with respect to various surface characteristics.

6.3.1 Surface Orientation: Horizontal vs. Vertical

The effect of gravity contributes to the major difference in terms of particle deposition flux onto surfaces of various orientations, e.g., a horizontal upward-facing surface (floor) as opposed to a vertical (wall) or a horizontal downward-facing surface (ceiling). Briefly, the mechanism of gravitational settling is primarily responsible for particle deposition onto the floor, while turbulent and Brownian diffusions are dominant deposition processes to walls and ceiling. Particle flux with respect to surfaces of various orientations can only be studied by means of spatially resolved deposition velocity measurements as described in Subsection 5.2.

Byrne *et al.*[49] employed the NAA technique to recover the particle mass deposited on various surfaces under forced convection in their cubic test chamber ($2 \times 2 \times 2$ m^3). They reported that proportionately more of the overall particle deposition flux was found on the floor (and thus less on walls) as particle size increases, as summarized in Table 3.

Thatcher *et al.*[46] used fluorescent tracer particles to measure particle deposition velocity with respect to different surfaces under natural convection flow conditions in their cubic enclosure ($1.2 \times 1.2 \times 1.2$ m^3). In addition to examining the effect of different surface orientations, the interior surface temperatures of the chamber were independently controlled at fixed surface-to-air temperatures to investigate the thermophoretic effects on particle deposition (see Subsection 6.3.3 for more discussion). In brief, the experimental chamber was heated on the floor and one vertical wall, and cooled on the ceiling and the opposite wall. As long as the surface-to-air temperature difference is kept identical, the thermophoretic effect is considered to be very similar, allowing comparisons to be made concerning particle deposition on surfaces of different orientations.

Table 3. Relative Contributions of Particle Deposition Flux Experimentally Determined for the Horizontal and Vertical Surfaces as a Function of Particle Diameter in Byrne *et al.*[49]

Particle size (μm)	Flux on horizontal surface (floor)	Flux on vertical surface (one wall)	Average deposition velocity* (m/s)
0.7	57%	9%	4.1×10^{-5}
2.5	68%	8%	6.2×10^{-5}
4.5	72%	7%	1.1×10^{-4}
5.4	80%	5%	2.0×10^{-4}

* accounted for particle deposition to all chamber surfaces.

Figure 6 presents a comparison of particle deposition velocity experimentally obtained from vertical and horizontal surfaces at the same temperature [+1.5K in (a) and –1.5K in (b) relative to the air temperature]. One of the distinctive features in Figure 6(a) is that particle deposition velocity onto the horizontal upward-facing surface (i.e., floor) increases as particle size increases, in agreement with theoretical predictions and experimental results in Byrne *et al.*[49] Also note in Figure 6 (a) that the measured deposition velocities onto vertical surfaces (i.e., wall), were increasingly lower than those on the floor by 1 to 3 orders of magnitude with the increase of particle size. Due to the diminishing contribution from gravitational settling, the deposition velocity to the horizontal downward-facing surface (i.e., ceiling) also decreases for increasing particle size, as shown in Figure 6(b).

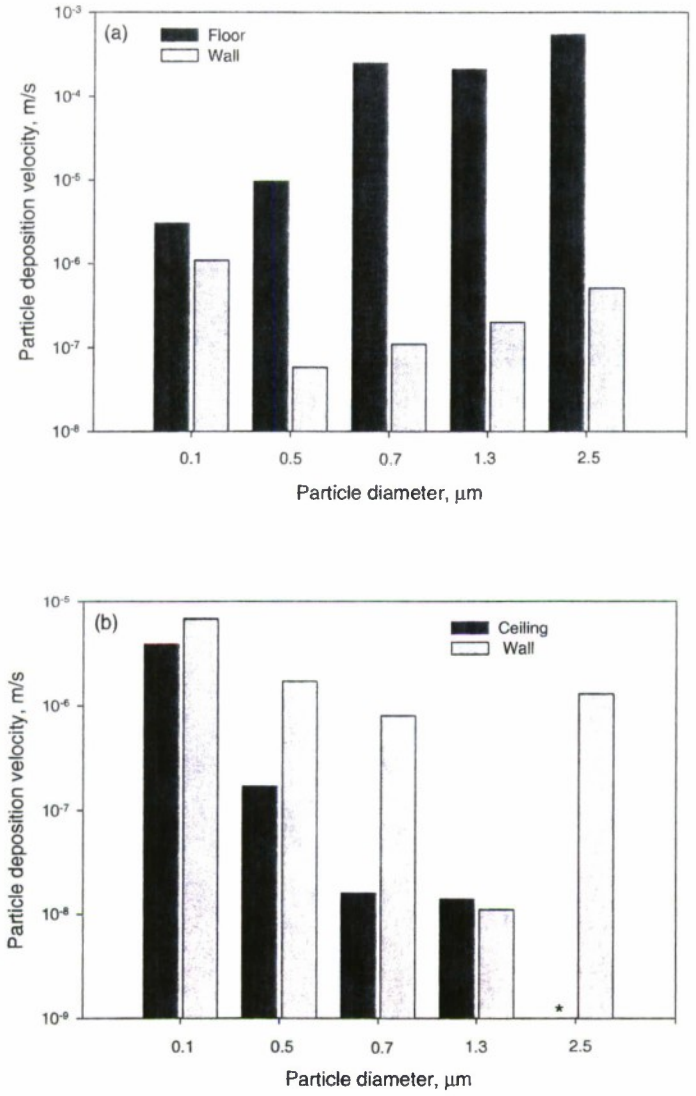

Figure 6. Comparison of experimentally measured deposition velocity for surfaces of various orientations in a cubic chamber under natural convection. The surface temperatures in (a) and (b) were kept at 1.5K higher and 1.5K lower than that of air, respectively. The values of deposition velocity plotted here were obtained from Table 2 in Thatcher *et al.*[46] The symbol of * in (b) denotes that the deposited particle mass on the ceiling was under the detection limit.

6.3.2 Surface Texture: Smooth vs. Rough

Surface texture complicates the process of particle deposition. The microscale roughness elements can alter the near-surface turbulent structures and reduce the boundary layer thickness, which, in turn, influences particle deposition. Roughness can also influence diffusive deposition even when the fluid-mechanical properties are not disturbed. The roughness elements can extend into and across the particle concentration boundary layer (which can be much thinner than the viscous sublayer), and this can expose the elements to higher particle concentration, thus enhancing the deposition rate. In addition, particle deposition may be further enhanced by more sites within the roughness elements available for impaction provided that particle inertia is sufficient. Experimental data regarding the effect of surface roughness on particle deposition within an enclosure are sparse. Nonetheless, a large collection of literature exists for particle deposition onto smooth and rough *pipe* walls, allowing some clues to be inferred. Sippola[15] provides an excellent review of this issue.

Based on some assumptions and the measurements from a stirred 2.6-L cylindrical chamber, Shimada *et al.*[60] proposed a semi-empirical model to explain the dependence of surface roughness height on particle Brownian and turbulent diffusive deposition, and to estimate the rate of particle deposition. Figure 7 illustrates the influence of surface roughness level on the experimentally measured deposition rates for 0.01–0.2 μm particles under the same turbulent mixing conditions (500 rpm). They concluded that as the surface roughness becomes significant, particle deposition tends to be influenced by the turbulent diffusion very close to the surface, leading to the enhancement of particle deposition. Later, Shimada *et al.*[62] further refined the model, and reported that the experimentally determined deposition rates agreed well with those reproduced in model calculations when the two-dimensional configuration of surface roughness was taken into account in calculating particle concentration above a rough surface. Since their modeling approach focused on diffusive deposition of0.01–0.2 μm particles, the mechanisms of gravitational settling and inertial impaction were not included.

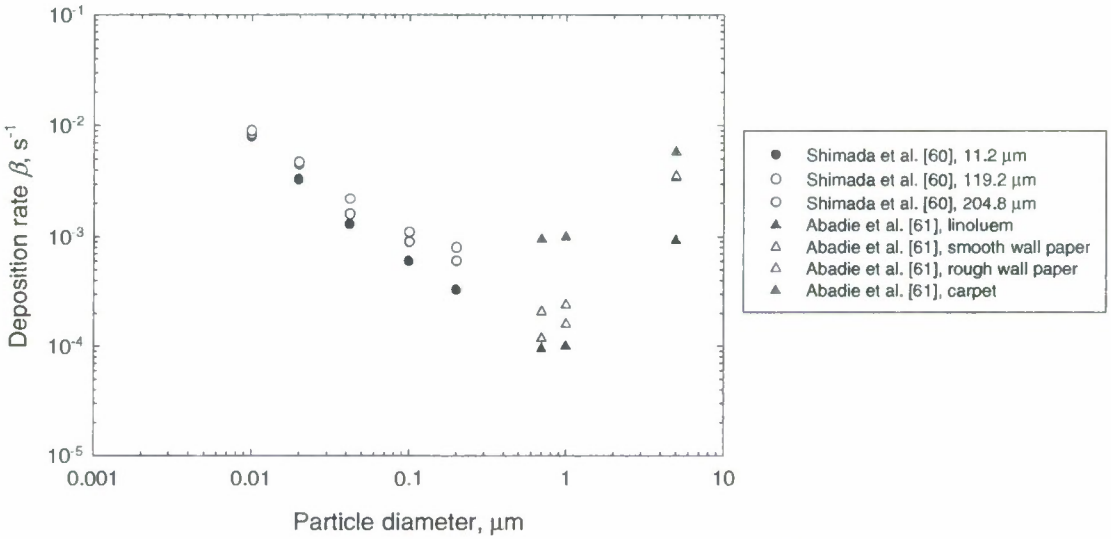

Figure 7. The dependence of experimentally measured particle deposition rates on the surface roughness. The length scale of 11.2, 119.2, and 204.8 μm in Shimada *et al.*[60] refers to the average height of roughness of the sandpapers placed on the interior surface of the enclosed tank. The S/V ratios of the experimental chamber in Shimada *et al.*[60] and Abadie *et al.*[61] are 47 and 10 m^{-1}, respectively.

Thatcher and Nazaroff[47] studied the influence of different surface roughness on particle deposition under natural convection in a 1.8 m^3 cubic enclosure. They found that deposition of small particles (~0.2 μm) was relatively insensitive to surface textures, but more pronounced effects were observed with increasing particle size. In their experiments, the measured deposition onto the roughest *vertical*[*] surface for 1.3 μm particles was 5 times greater than deposition to a vertical smooth surface. They also noted that the surface roughness had more substantial effects for vertical surfaces than horizontal, and for warm surfaces than cool.

Various wall treatments on all interior surfaces were furnished in a cubic chamber ($0.6 \times 0.6 \times 0.6$ m^3) to measure deposition rates in Abadie *et al.*[61] for particles of 0.7, 1.0, and 5.0 μm under fan mixing conditions. As shown in Figure 7, the measured particle deposition rates were found to increase with the following order of increasing surface roughness level: linoleum, smooth wall paper, rough wall paper, and carpet.

Lai *et al.*[63] conducted deposition experiments in an 8-m^3 test chamber under different fan speeds using monodisperse particles from 0.7 to 5.4 μm. They observed that, at the highest fan speed, the average ratio of particle deposition flux onto a *vertical* rough surface over smooth surface increased from 1.05 for 0.7 μm particles to 1.1, 1.6, and 2.4 for particle sizes 2.5, 4.3, and 5.4 μm, respectively. Since gravity does not play a role in particle deposition onto vertical walls, surface roughness and perhaps particle inertia for larger particles, are believed to contribute to the enhanced particle deposition in the experiments.

Thatcher *et al.*[64] reported on the influence of particle deposition rates upon different furnishing levels (bare, carpeted, and fully furnished with chairs, curtains, etc.) in a room-sized setting ($2.2 \times 2.7 \times 2.4$ m^3) for particle sizes from 0.5 to 10 μm. The use of carpeting and furniture can be considered to increase the average roughness of surfaces (although the airflow pattern will be different for the furnished scenario due to additional obstructions inside the room; also increased surface area to volume ratio). Across all particle sizes measured, the measured deposition rates were observed to have the consistently descending trend with respect to the furnishing or roughness level: furnished > carpeted > bare.

Lai and Nazaroff[48] placed glass plates and sandpapers of different grades on the *vertical* walls of a 1.8-m^3 cubic chamber to measure the deposition velocities of supermicron particles under forced convection conditions. They reported that the experimentally determined deposition velocity appeared to reach a fairly steady value for particles larger than 7 μm. In addition, the deposition velocity was observed to increase with increasing roughness grade, albeit the increments with increasing surface roughness were not as significant as the influence of particle size on deposition.

6.3.3 Surface Temperature: Warm vs. Cold

As discussed in Subsection 3.5, thermophoretic forces on airborne particles can be induced by temperature differences between a surface and air. In the presence of a temperature gradient, particles always move toward the direction of lower temperature. As a consequence, particles tend to preferentially deposit onto a cold surface over a warm one due to thermophoresis.

[*] Vertical surfaces are studied to exclude the direct influence of gravity on deposition.

Numerous experimental studies have examined the effectiveness of exploiting thermophoresis to minimize particle deposition on silicon wafers for microcontamination control.[17–19] However, experimental data for particle deposition on cold and warm surfaces with respect to an enclosed volume are sparse. The experiments performed by Thatcher *et al.*[46] provided valuable insights into particle deposition under the influence of surface-to-air temperature differences within an enclosure. Figure 8 represents the experimentally measured deposition velocity to the *vertical* surfaces as a function of the

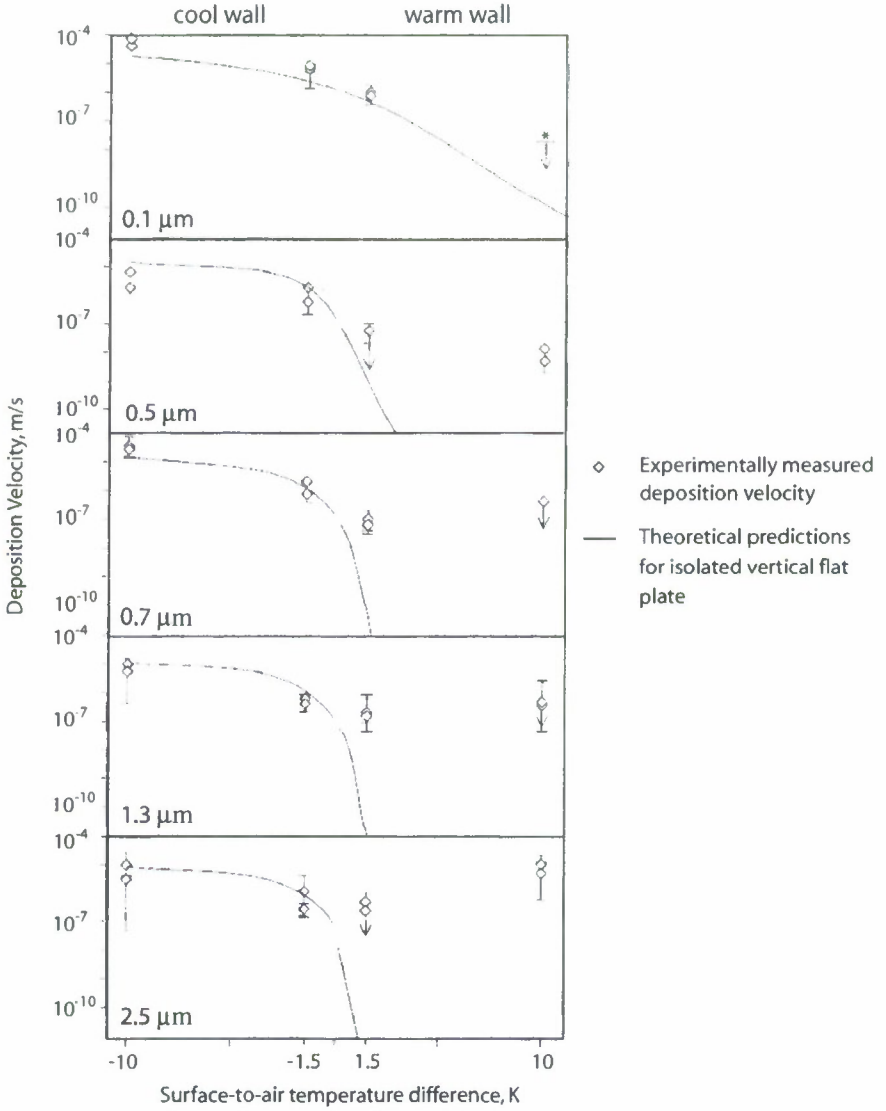

Figure 8. Experimentally measured deposition velocities to the vertical walls of a $1.2 \times 1.2 \times 1.2$ m^3 enclosure as functions of particle diameter and surface-to-air temperature difference (reprinted with permission from Thatcher *et al.*[46] Deposition velocities predicted theoretically by Nazaroff and Cass[65] for a vertical isolated flat surface are also plotted for comparison. Each diamond symbol represents the average value obtained by 10 local surface extractions over the central portion of the cool or the warm wall from a single experiment. The error bars span the maximum and minimum values of measurements at each location, while an arrow is used to indicate that the lower limit of the 95% confidence interval for the mean was less than the detection limit. The symbol * denotes that the deposited particle mass was under the detection limit.

surface-to-air temperature difference (±1.5K and ±10K, respectively) for five different particle sizes. The deposition velocity predicted theoretically by Nazaroff and Cass[24,65] was also plotted for comparison.

As shown in Figure 8, the thermophoresis effect on deposition velocity appears to be diminishing as particle size increases. For instance, the experimentally obtained deposition velocity to the cool vertical surface (–10K) for 0.1 μm particles is more than 3 orders of magnitude higher than to the warm vertical surface (+10K). On the other hand, the measured deposition velocities to the cool and warm walls for larger particles (1.3 and 2.5 μm) are approximately the same. Furthermore, for particles larger than 0.5 μm, the measured deposition velocity on the warm wall at +10K is higher than at +1.5K. This observation is counterintuitive since a warmer surface is anticipated to enhance thermophoretic repulsion thus reducing particle deposition.

In summary, the deposition velocity determined experimentally in Thatcher *et al.*[46] shows relatively good agreements with the predictions for all five particle sizes studied when the wall surface temperature is cooler than the air. In contrast, the deposition velocity to the warm wall obtained in the experiments appears to be much higher than predicted, particularly for increasing particle size. The discrepancy between experimental findings and theoretical predictions may be attributed to the fact that the existing model does not account for all the factors influencing particle deposition under the settings of the experiments. The surface-to-air temperature difference influences not only particle thermophoretic velocity, but also the near-surface airflow pattern, which further introduces more complexities toward understanding of the deposition processes. The complicated airflow pattern and flow instability in their chamber experiments are believed to play a role in contributing the variations of the deposition velocity measurements. Other factors such as particle inertia and the effect of corners on airflow not being addressed in the model may be of importance to influence the deposition process.

6.3.4 In the Presence of an Electric Field

Electrostatic forces may play an important role in influencing particle deposition. When the interior surface of an enclosed volume has the tendency to acquire electrostatic charge (e.g., made of poor conducting materials), a local near-surface electric field may develop, which, in turn, enhances the deposition of charged particles.* Early experiments have shown that the presence of electric charges on surfaces can introduce additional variability to particle deposition measurements.[66]

McMurry and Rader[67] demonstrated in their 60-m^3 Teflon chamber experiments under natural convection that the enhanced deposition for 0.07–1 μm particles was attributed to electrostatic effects, as seen in Figure 9. In another set of Teflon film bag (250 L) experiments, the deposition rates of singly charged particles could be significantly increased as compared to particles at Boltzmann distribution,[67] as shown by the symbols ∇ and ▼ in Figure 10. For instance, a nearly 30 times deposition enhancement was observed for the 0.1 μm singly charged particles in comparison to particles with Boltzmann charge distribution. In addition, their experimental data indicated that the deposition rates

* As mentioned in Subsection 3.6, airborne particles become charged by collision with air ions and carry certain charges depending on their particle size according to Boltzmann distribution.

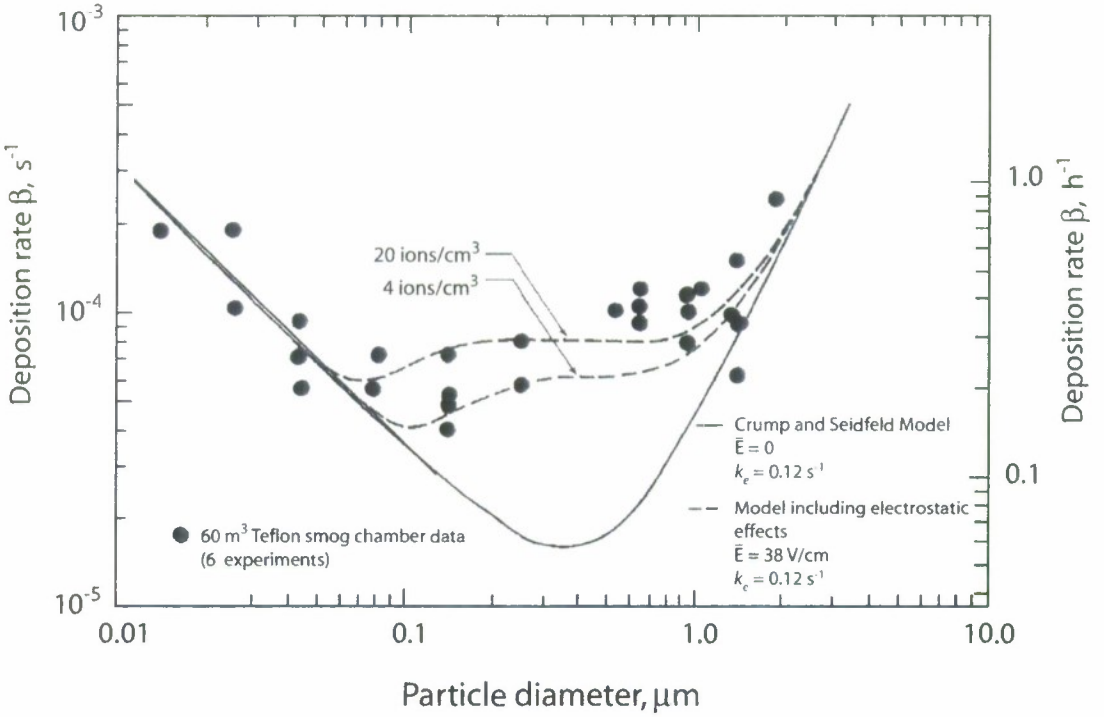

Figure 9. Comparison of measured particle deposition rates in a 60 m^3 Teflon smog chamber with modeling predictions by Crump and Seinfeld.[68] $\bar{E}$ and k_e denote the estimated average electric field strength on the chamber interior surface and the parameter of airflow turbulence intensity, respectively. Note that the experimental data exceeded predicted values for 0.07–1 μm particles when electrostatic effects were not taken into account. Reprinted with permission from McMurry and Rader.[67]

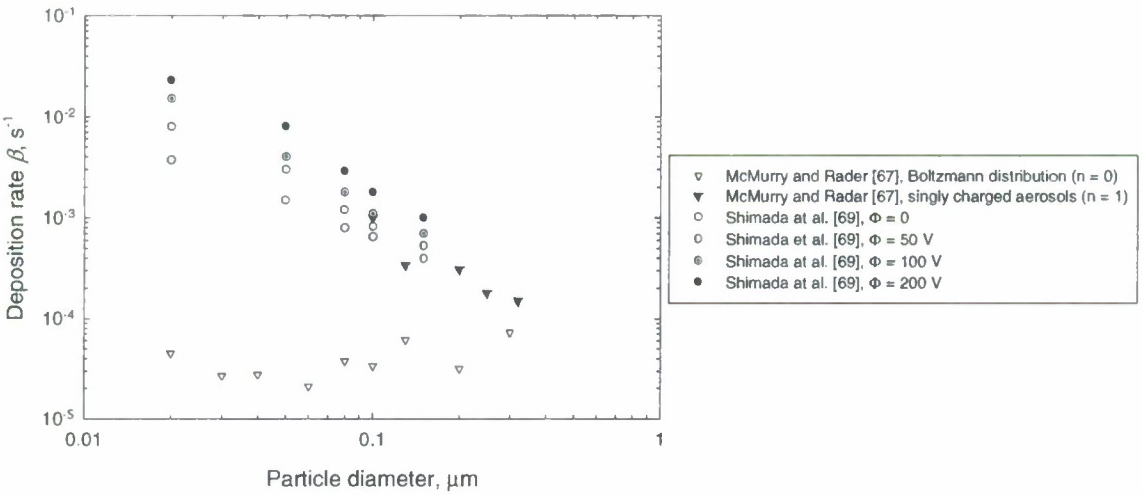

Figure 10. Experimentally determined particle deposition rates as a function of particle diameter under various influences of electrostatic attractions. The data points of MuMurry and Rader[67] were obtained in a 250-L Teflon film bag (natural convection; S/V = 10.6 m^{-1}), in which the average electric field was estimated as 45 V/cm via data fitting to their model. The electrostatic attractions in Shimada *et al.*[69] were established by applying known voltage (Φ) at the bottom of the enclosed tank (forced convection; S/V = 47 m^{-1}).

were nearly identical for oppositely charged particles of the same size. The laboratory results agreed satisfactorily with their model that incorporated electrostatic drift as an additional transport mechanism. As explained in the model, deposition for particles larger than 1 μm and smaller than 0.05 μm were still dominated by gravitational settling and Brownian/turbulent diffusion, respectively; while electrostatic effects were important factors influencing deposition of 0.05–1 μm particles.

Shimada *et al.*[69] performed deposition measurements for 0.02–0.2 μm particles in a stirred metal tank where the turbulence intensity and the electric field could be controlled. They found no difference in deposition rates for charged and uncharged particles when the surfaces were grounded. As the electric field strength increased, however, the enhancements of particle deposition rates were observed, as indicated in Figure 10.

By directly collecting particle deposition mass onto vertical surfaces in a 1.8-m^3 cubic chamber, Lai[70] reported that the measured particle deposition velocities onto acetate sheets for 3.5–9 μm particles were more than an order of magnitude higher than those onto glass and copper plates, owing to the electrostatic effects. The laboratory data indicated that deposition velocities for both glass and copper surfaces were comparable, and the use of anti-electrostatic spray on the surfaces was found to lead to reduced particle depositions by minimizing the Coulombic effect.

7. Modeling Particle Deposition and Experimental Validations

Two major types of models, both theoretical-based and semi-empirical, have been proposed to quantify, predict, and explain particle deposition in enclosures. The first type, as will be discussed in Subsections 7.1 and 7.2, involves first modeling the air turbulent structure adjacent to the enclosure surfaces, and particle transport is subsequently formulated accounting for gravity, diffusion, and other deposition mechanisms. One key challenge in this modeling approach lies in the determination of the near-surface particle eddy diffusivity, which is postulated to be related to the air turbulence intensity within the enclosure as well as the distance to the wall. The second type of modeling approach, as will be described in Subsection 7.3, applies the well-known analogy between mass and heat transfer, and deposition rate of particles from the gas phase to the surface due to diffusion is estimated via the mass transfer correlation.

In this section, the modeling developments based on these two approaches for predicting particle deposition rates in enclosures are summarized, together with the available experimental investigations to compare against the modeling analyses as well as the limitations associated with these models.

7.1 Homogeneous Turbulence Model

Modeling efforts for studying particle deposition from turbulent flow onto enclosure surfaces were initiated in the early 1950s. Corner and Pendlebury[53] developed the first theoretical model accounting for particle deposition onto the surfaces of horizontal and vertical orientations in a rectangular enclosure where the air was homogeneously turbulent. Their model was derived based on the following key assumptions: (1) the air outside the boundary layer is homogeneously turbulent, and aerosol concentration is uniform (as illustrated in Figure 1); (2) within the boundary layer of thickness δ, the fluid motion is turbulent with random fluctuations, but the mean fluid motion is parallel to the surface; (3) the velocity gradient is linear within the boundary layer; (4) the mechanisms of gravitational settling, Brownian/turbulent diffusion are responsible for particle transport through the boundary layer; (5) turbulent diffusion dominates Brownian motion at the edge of the boundary layer; and (6) particle transport is quasi-steady-state in the boundary layer.

Under the above assumptions, the aerosol concentration in the boundary layer adjacent to the surface is governed by

$$\frac{\partial}{\partial y}\left[\left(\varepsilon_p + D\right)\frac{dC}{dy}\right] - v_{ts}\mathbf{k}\cdot\frac{\partial C}{\partial y} = 0, \tag{21}$$

where $\mathbf{k}$ is the unit normal vector in the vertical direction. The first and second terms of Eq. (21) account for the processes of turbulent/Brownian diffusion and gravitational settling, respectively. The boundary conditions for the above equation are

$$C = 0 \quad \text{at } y = 0$$

$$C = C_\infty \text{ at } y \geq \delta \tag{22}$$

where C_∞ is the bulk aerosol concentration outside the boundary layer. The particle concentration profile in the boundary layer can thus be solved from Eqs. (21) and (22). In the Corner and Pendlebury model, the particle eddy diffusivity is approximated using Prandtl's mixing length theory as

$$\varepsilon_p = k_e y^2, \tag{23}$$

where k_e is the turbulence intensity parameter used to characterize the degree of turbulent mixing inside the enclosure. There is no a priori way to estimate the values of k_e with available data; hence, it is usually determined empirically by fitting experimental data into the theory. Corner and Pendlebury[53] suggested that k_e be evaluated as

$$k_e = \kappa \frac{dU}{dy}, \tag{24}$$

where κ is the von Kármán's constant (usually taken as 0.4), and U is the component of the mean flow velocity parallel to the surface. The velocity gradient, dU/dy, is approximated by means of fluid drag force balance for a flat plate in Corner and Pendlebury's model.

Following the seminal work of Corner and Pendlebury,[53] several additional model extensions have been proposed. Crump and Seinfeld[68] derived expressions for estimating particle deposition rate in an enclosure of arbitrary shape, and the analytical solutions for a spherical vessel were specifically formulated. They showed that, in an enclosure having only horizontal and vertical surfaces, the transport processes of gravitational settling and diffusion can be treated independently by vectorially summing the gravitational settling velocity to the deposition velocity associated with the diffusion process. For the inclined surfaces of a sphere, however, their derivations indicated that these two mechanisms are always intimately coupled to each other and cannot be separated. They proposed that the value of k_e can be evaluated from the fluid energy dissipation rate, instead of velocity gradient in the boundary layer as suggested in Corner and Pendlebury.[53] Moreover, Crump and Seinfeld[68] derived the particle deposition rate with a more general form of $\varepsilon_p = k_e y^n$, where n can be any number, which could be obtained by empirically fitting experimental data. They also demonstrated that the use of the exponent n = 3, as suggested by Friedlander,[27] could produce analytical expressions to predict deposition that are analogous to those with n = 2.

In summary, Crump and Seinfeld[68] calculated the particle deposition velocity onto the surface of an enclosure to be

$$v_d(\theta) = \frac{v_{ts}\cos\theta}{\exp\left[\pi v_t \cos\theta \Big/ \left(n \sin\frac{\pi}{n}\right)\sqrt[n]{k_e \varepsilon_p^{\,n-1}}\right] - 1}, \qquad (25)$$

where v_{ts} is the particle terminal settling velocity, and θ is the angle between normal vector of wall and gravity direction (rad).

To validate their own theoretical derivations, Crump *et al.*[71] performed particle deposition experiments in a spherical vessel. By fitting the data and using n = 2, the turbulence intensity parameter k_e in their study was evaluated in terms of the volumetric air flowrate into the chamber, which was related to the turbulent energy dissipation rate, as suggested in Okuyama *et al.*[72*] The experimental results in Crump *et al.*[71] showed good agreement with the analytical expressions with respect to the dependence of particle deposition rates on particle size and turbulence intensity.

Based on the existing model developed by Crump and Seinfeld,[68] McMurry and Rader[67] incorporated electrostatic effects as an additional particle deposition mechanism to evaluate the particle deposition rate in an enclosure. Experiments were also performed to measure the deposition rate of neutral and singly charged aerosols in a 250-L Teflon bag and a 60-m^3 Teflon smog chamber, respectively. A good fit between the experimental results and the model predictions was obtained by setting n = 2 and adjusting the values for k_e and the mean electric field.

Okuyama *et al.*[23] studied the deposition loss of monodisperse aerosols with particle diameters of 0.006 to 2 μm in a stirred cylindrical vessel. The turbulence intensity parameter k_e in their experiments was calculated by the average energy dissipation rate per unit mass of air, and the parameters of κ and n were obtained by fitting the experimental data. The experimental deposition rates compared well with the model calculations by Crump and Seinfeld[68] when the eddy diffusivity was assumed to be proportional to the 2.7th power of the distance from the surface (i.e., n = 2.7). In addition, more deviations from the model were observed for increasing particle size or flow turbulence intensity, and this is likely attributed to effects of enhanced particle inertia, which was not considered in the model.

Cheng[56] measured the particle deposition rates of monodisperse particles ranging from 0.005 to 2 μm in a spherical chamber. Both the chamber temperature and air velocity profiles under various turbulence conditions were measured. The turbulence intensity in the experiments evaluated using both methods, including the velocity gradient as shown in Eq. (24) and energy dissipation rate,[23, 72] gave reasonable estimates of k_e as well as the particle deposition rates. The data were well explained by Crump and Seinfeld's model,[68] except that the best-fitted estimate of n was approximately 2.8, instead of n = 2 as supported in Crump *et al.*,[71] McMurry and Rader,[67] and Chen *et al.*[42]

---

* The expression $k_e \propto (\varepsilon/\nu)^{1/2}$ suggested in Okuyama *et al.*[72] originates essentially from the Prandtl's mixing length formula, where $(\varepsilon/\nu)^{1/2}$ is proportional to the r.m.s. velocity gradient in the boundary layer. The symbol ε refers to the turbulence energy dissipation rate and ν is the kinematic viscosity of the fluid.

By vectorially adding the deposition flux, Nazaroff and Cass[65] incorporated the thermophoresis effect into the model by Corner and Pendlebury[53] to estimate deposition velocity onto a vertical isolated flat plate in the presence of surface-to-air temperature difference. Their analysis showed that, as particle size increases, an increasingly pronounced difference in deposition velocity is predicted for the vertical warm relative to the cool walls. The experimental findings in Thatcher *et al.*[46] indicated that the model appeared to greatly underestimate the deposition velocity for a warm surface, especially for supermicron particles, as was explored in Subsection 6.3.3.

In summary, the existing experimental data agree reasonably well with the theory by Corner and Pendlebury,[53] including its extensions. However, there are still some issues that must be carefully examined before applying the model to various scenarios. For example, can k_e and n be determined in any particular enclosure, without resorting to fitting the results of sophisticated particle deposition experiments? These two parameters are key and vary with experimental conditions; they ultimately influence the magnitude of the particle eddy diffusivity ε_p, which directly affects the calculation of deposition rate and flux to the surface.

Table 4 summarizes the values of n and k_e determined from various particle deposition experiments. The scenario of n = 2 is regarded as the "classical" form of Corner and Pendlebury[53] and Crump and Seinfeld.[68] This is also supported by some experimental data (Crump *et al.*;[71] McMurry and Rader;[67] Chen *et al.*[42]). In other experimental findings, however, the best fit of the data to the model occurs at n = 2.6–2.8 (Okuyama *et al.*;[23] Van Dingenen *et al.*;[57] Holub *et al.*;[73] Cheng,[56]), close to n = 3 as suggested by Friedlander[27] as well as Pandian and Friedlander[74] based on a theoretical perspective of the analogy between mass and heat transfer.

In the definition of particle eddy diffusivity (in $cm^2 s^{-1}$, $\varepsilon_p = k_e y^n$) when n = 2, the dimension of k_e (s^{-1}) has the dimensions of a rate constant. Non-integer values of n leads to k_e with a dimension of $L^{2-n}T^{-1}$, which not only lacks a solid physical foundation but also causes conceptual and practical problems when k_e is to be evaluated based on information of velocity gradient or turbulent energy dissipation rate (both methods assuming n = 2). Based on the rules of dimensional analysis, Beneš and Holub[75] suggested a modified formulation to avoid the dimensional inconsistency problem:

$$\varepsilon_p = k_e \delta^2 \left(\frac{y}{\delta} \right)^n , \tag{26}$$

where δ is the boundary layer thickness. Using this new expression has shown to yield good agreements with data from one experimental study.[56] However, it remains unresolved with respect to the evaluation method for n.

Nevertheless, Crump and Seinfeld[68] noted that the choice of n value is of little importance from the standpoint of their theoretical derivations. Van Dingenen *et al.*[57] suggested that, after re-examining the data by Crump *et al.*[71] and McMurry and Rader,[67] the exact value of n is trivial as long as an appropriate k_e is determined in an independent way, for instance, the evaluation of energy dissipation rate or near-surface velocity gradient, as suggested in Okuyama *et al.*[72]

Table 4. Summary of the Values of n and k_e Determined from Various Particle Deposition Experiments

n	k_e, s^{-1}	Method to evaluate k_e	Flow mixing method	Experimental chamber	Particle size (μm)	Investigators
2	0.028 and 0.068 for two flowrates	data fitting and later correlated k_e to flowrates	convective mixing by feeding air continuously	spherical glass vessel, 118 L	0.024 to 0.794	Crump et al., 1983[71]
2	6.4×10^{-3} for 250 L bag and 0.12 for 60 m^3 smog chamber	data fitting	natural convection	250 L Teflon film bag and 60 m^3 Teflon film smog chamber	0.02 to1.8	McMurry and Rader, 1985[67]
2	0.004 and 0.02 at ΔT = 0 and 10°C	data fitting	convective mixing by temperature gradient	Pyrex glass cylinder, 165 L	0.04-3.0	Chen et al., 1992[42]
2.6	3.5×10^{-2}	data fitting	natural convection	spherical boro-silicate glass chamber, 230 L	0.02 to 0.2	Van Dingenen et al., 1989[57]
2.6	7.1×10^{-3}	data fitting	natural convection	spherical glass chamber, 0.23 m^3	0.001-0.3	Holub et al., 1988[73]
	107		turbulent mixing by fan	cylindrical chamber, 3.9 m^3		
2.7	ranging from 0.05 to 264, depending on the fan speeds	estimated from fluid energy dissipation; assuming κ = 0.3	turbulent mixing by fan and natural convection	cylindrical tank, 2.6 L	0.006 to 2	Okuyama et al., 1986[23]
2.8	0.0152 to 1.0 depending on the fan speeds	(1) velocity gradient near the chamber surface; (2) energy dissipation by mixing; and (3) data fitting	turbulent mixing (fan) and natural convection	spherical aluminum chamber, 161 L	0.005 to 2	Cheng, 1997[56]

7.2 Three-Layer Model

Incorporating the information on the structure of near-surface turbulent diffusivity, Lai and Nazaroff[25] proposed a model in which only one parameter, friction velocity, u^*, is required to evaluate particle deposition under homogeneously turbulent conditions. The friction velocity is defined by

$$u^* = \left(\frac{\tau_w}{\rho_a}\right)^{1/2} = \left(\nu \left.\frac{dU}{dy}\right|_{y=0}\right)^{1/2}, \tag{27}$$

where τ_w is the shear stress at the surface, ρ_a is the air density, and ν is the kinematic viscosity of air. The parameter u^* is intended to capture the turbulent characteristics in the vicinity of the surface. As suggested in Eq. (27), the friction velocity is related to the velocity gradient at the surface, dU/dy, which can be evaluated by a freestream air speed U_∞ and a characteristic length of enclosure surfaces L:[76]

$$\left.\frac{dU}{dy}\right|_{y=0} = \left(\frac{0.074}{\rho_a \nu}\right)\left(\frac{\rho_a U_\infty^2}{2}\right)\left(\frac{U_\infty L}{\nu}\right)^{-1/5}. \tag{28}$$

Another approach of estimating friction velocity is to measure the velocity profile in the logarithmic flow region near the surface, i.e., the Clauser-plot method.[77] Within the turbulent boundary layer, the time-averaged velocity, U, as a function of distance from the surface y is expressed by

$$\frac{U}{U_\infty} = \frac{2.5u^*}{U_\infty} \ln\left(\frac{yU_\infty}{\nu}\right) + A, \tag{29}$$

where A is a constant. Thus, the friction velocity can be inferred from the slope of the line by plotting measurements of U/U_∞ versus the logarithm of (yU_∞/ν).

Commonly known as the *law of the wall*, a turbulent boundary layer consists of three distinct zones according to the velocity distribution as a function of the distance perpendicular to the wall.[76] The approach used by Lai and Nazaroff[25] to analyze particle deposition from turbulent flow is to examine the turbulent flow structure zone by zone, and to formulate particle transport equations for each zone, assuming (1) gravitational settling and Brownian and turbulent diffusion are responsible for the particle deposition processes; (2) constant particle flux in the concentration boundary layer; (3) particle eddy diffusivity well represented by fluid turbulent viscosity; and (4) negligible surface roughness effects. Across the boundary layer, the expression for the deposition velocity was then integrated for each zone. The deposition velocity was evaluated for vertical, upward, and downward horizontal surfaces, and the first-order deposition rates were provided for rectangular and spherical cavities, respectively. This approach is somewhat complicated, but remains practical to use.

Table 5 summarizes the equations required for calculating particle deposition along with explanations of parameters used in the model. Their model predictions compared well with published experimental data for deposition of 0.001–2 μm particles in a spherical enclosure (Cheng[56]), as seen in Figure 11. Lai and Nazaroff[25] indicated that their model calculations yield the best agreement with the model by Crump and Seinfeld[68] with n = 2.95, very close to n = 3, which is used to characterize convective heat transfer.[74] It is expected that the analogy between heat and mass transfer should hold when particle inertia is insignificant.

Table 5. Summary of Equations Used for Particle Deposition Analysis in the Three-Layer Model (reprinted with permission from Lai and Nazaroff[25])

Parameters	Equations
Integral I[¥]	$I = \left[3.64Sc^{2/3}(a-b)+39\right]$ $a = \frac{1}{2}\ln\left[\frac{\left(10.92Sc^{-1/3}+4.3\right)^3}{Sc^{-1}+0.0609}\right]+\sqrt{3}\tan^{-1}\left[\frac{8.6-10.92Sc^{-1/3}}{\sqrt{3}\,10.92Sc^{-1/3}}\right]$ $b = \frac{1}{2}\ln\left[\frac{\left(10.92Sc^{-1/3}+r^+\right)^3}{Sc^{-1}+7.669\times10^{-4}\left(r^+\right)^3}\right]+\sqrt{3}\tan^{-1}\left[\frac{2r^+-10.92Sc^{-1/3}}{\sqrt{3}\,10.92Sc^{-1/3}}\right]$
Deposition velocity vertical surface	$v_{d,v} = \frac{u^*}{I}$
Deposition velocity upward horizontal surface	$v_{d,u} = \frac{v_{ts}}{1-\exp\left(-\frac{v_{ts}I}{u^*}\right)}$
Deposition velocity downward horizontal surface	$v_{d,d} = \frac{v_{ts}}{\exp\left(-\frac{v_{ts}I}{u^*}\right)-1}$
Deposition rate, rectangular enclosure	$\beta = \frac{v_{d,v}A_v + v_{d,u}A_u + v_{d,d}A_d}{V}$
Deposition rate, spherical enclosure[†]	$\beta = \frac{3}{2R}\left(\frac{u^*}{I}\right)\left[2D_1(x)+\frac{1}{2}x\right]$ where $x = \frac{v_{ts}I}{u^*}$

Nomenclature:

$Sc = \nu/D$ = particle Schmidt number
ν = kinematic viscosity of air
D = Brownian diffusivity of particles
$r^+ = d_p u^*/2\nu$
d_p = particle diameter
u^* = friction velocity
v_{ts} = terminal settling velocity of particles
A_v = area of vertical surfaces
A_u = area of upward-facing surfaces
A_d = area of downward-facing surfaces
V = room volume
R = radius of spherical enclosure
$D_1(x)$ = Debye function defined by

$$D_1(x) = \frac{1}{x}\int_0^x \frac{t}{e^t-1}dt$$

[¥] The integral is evelueted anelytically under the approximation thet Brownian diffusivity, D, is negligible compared with eddy diffusivity for $y^+ \geq 4.3$, where y^+ is the normalized distance from the surface. This epproximation is accurete to 1% or better for particle diameters larger than 0.01 μm. For smaller particles, the integretion must be carried out numerically. See the following for results.

Particle diameter, d_p (μm)	Integral, I (-)
0.001	29.1
0.0015	49.1
0.002	71.0
0.003	120.3
0.004	174.9
0.005	234.2
0.006	297.4
0.007	364.0
0.008	432.7
0.009	504.5
0.01	579.3

† In the limit of small particles (negligible influence of gravitational settling), the expression simplified to $\beta = 3u^*(RI)^{-1}$. In the limit of large particles (negligible influence of Brownian diffusion), the expression simplifies to $\beta = 3v_{ts}(4R)^{-1}$.

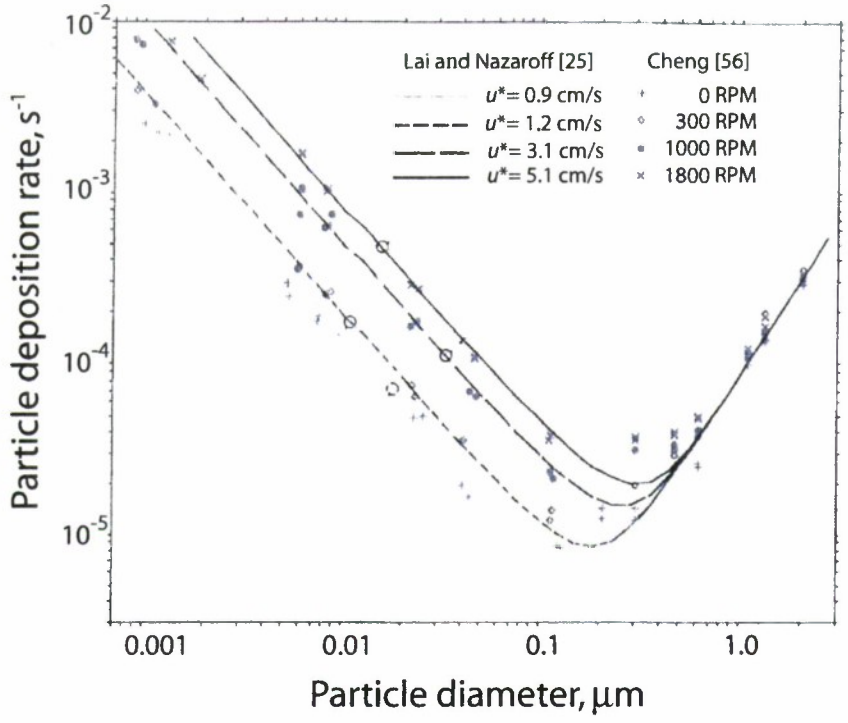

Figure 11. Predictions of particle deposition rate as a function of particle diameter in the three-layer model in Lai and Nazaroff[25] compared with experimental data (Cheng[56]). Reprinted with permission from Lai and Nazaroff.[25]

Lai and Nazaroff[48] performed laboratory experiments to measure deposition of 0.9–9 μm particles from turbulent flow onto vertical surfaces of a cubic aluminum chamber. The experimentally measured particle deposition velocities for 9-μm particles were higher by a factor of 30–150 as compared to their own model predictions for friction velocities of 2.9–9.8 m/s. The chamber walls were grounded; thus, electrostatic force was considered negligible. They note that the discrepancy between experimental observations and model calculations is attributed to the inadequacies of the model, in which the key transport and deposition processes for supermicron particles may not be addressed appropriately. For example, particle inertia and shear-induced lift force*

* A particle in a shear flow field may experience a lift force perpendicular to the main flow direction. This life force arises owing to particle inertia and is important for large particles. Lai and Nazaroff[45] postulated that shear-induced lift force may be important in their experiments, in which significant velocity gradient adjacent to the surface is expected owing to the parallel airflow pattern along the vertical walls of the chamber.

are postulated to be potentially important players to enhance transport of larger particles through the relatively thin boundary layers and lead to subsequent surface deposition.

Lai[78] later incorporated the mechanism of particle inertia into the three-layer model by adopting the commonly accepted electrical resistance analogy in atmospheric dry deposition modeling,[31] to simulate supermicron particle deposition from turbulent flow to a vertical surface. Treating the friction velocity as the fitting parameter and incorporating analyses accounting for surface roughness effects,[79] the agreements between experimental data and modeling calculations were good for smooth surfaces, but less satisfactory for rough surfaces.

The influence of electrostatic drift was considered as an additional particle deposition mechanism in the inertia-incorporated three-layer model by Chen and Lai.[80] The experimental findings involved with electrostatic effects in Lai[70] again demonstrated that the particle deposition is a complicated process, particularly when mechanisms more than diffusion and gravitational settling are involved. More detailed experiments or numerical simulation on near-surface airflow structure will be helpful to shed light on the dynamics of particle transport.

7.3 Mass Transfer Model

As mentioned in Subsection 4.1, particle deposition velocity is equivalent to a mass transfer coefficient with the units of length per time (LT^{-1}). Based on the analogies for mass and heat transfer,[81] the correlations for transfer coefficients in mass and heat transport should be of the same form for particle mass transfer from turbulent flow to the enclosure surfaces by diffusion, and for convective heat transfer in jacketed vessels, assuming that the average roughness heights are immersed within the viscous sub-layer (i.e., for smooth walls). Following this analogy, Pandian and Friedlander[74] proposed a semi-empirical mass transfer expression to estimate the rate of particle deposition due to turbulent and Brownian diffusion in the form of Sherwood-Reynolds-Schmidt correlation:

$$Sh = a(Re)^{2/3}(Sc)^{1/3}, \tag{30}$$

where Sh is the Sherwood number = $k_m D_c/D$, k_m is the mass transfer coefficient or particle deposition velocity (m s^{-1}), D_c is the chamber diameter (m), D is particle diffusivity (m^2 s^{-1}), Re is the Reynolds number for stirring = ND_s/ν, N is the impeller speed (rpm, revolutions per minute) in a stirred chamber, D_s is the stirrer diameter (m), ν is the kinematic viscosity of fluid in the chamber (m^2 s^{-1}), Sc is the particle Schmidt number = ν/D, and a is a constant.

By fitting the experimental data in Okuyama *et al.*[23] to Eq. (30), Pandian and Friedlander[74] obtained a = 0.63 as the best fit for particles smaller than 0.1 μm in diameter and Re no greater than 3000. Other laboratory results were also used to compare with Eq. (30), and good agreements were found, as shown in Figure 12. Using different sets of data, the values of fitted a have been found to be slightly different.

By equating the expression of particle deposition rate in Crump and Seinfeld[68] to Eq. (30), Cheng[56] showed that the mass transfer equation proposed by Pandian and Friedlander[74] has an equivalent form as the Crump and Seinfeld model with n = 3.

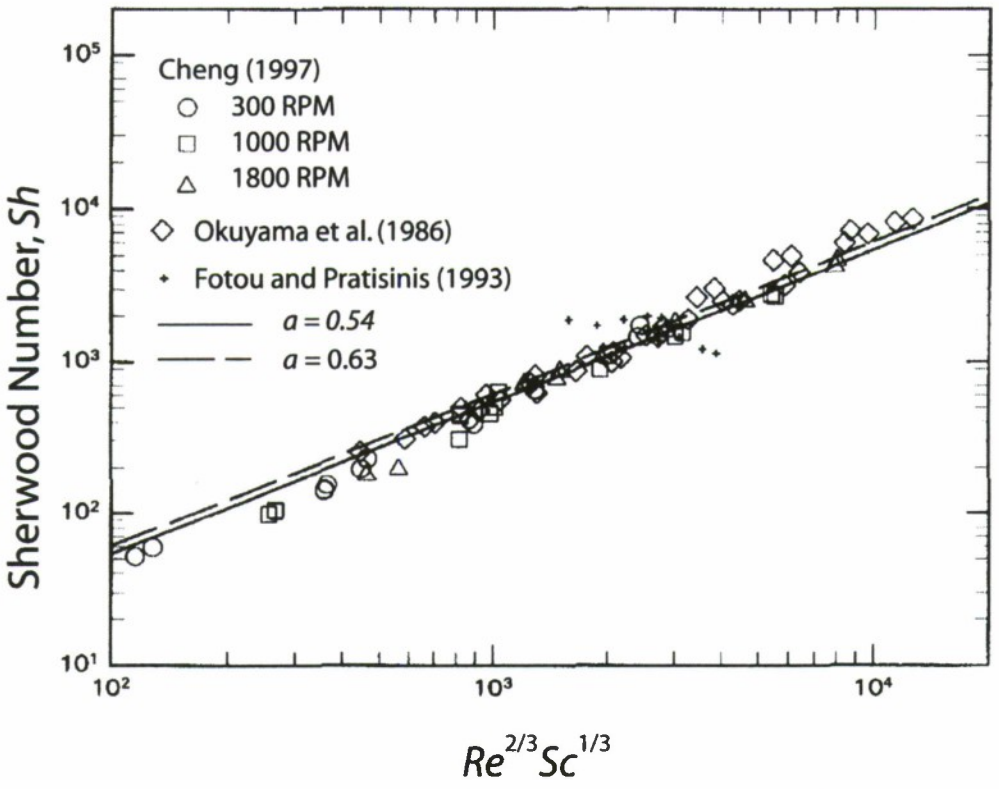

Figure 12. Mass transfer correlation of particle diffusional deposition in smooth walled stirred chamber, with Sherwood number (Sh) plotted as a function of $Re^{2/3}Sc^{1/3}$. The dash line of a = 0.63 was obtained from fitting the data in Okuyama *et al.*,[23] and the straight line of $a = 0.54$ was obtained from fitting the data in Okuyama *et al.*[23] and Cheng.[56] Reprinted with permission from Cheng.[56]

The particle deposition rate estimated from the mass transfer correlation thus can be estimated as

$$\beta = a\frac{D}{D_c}\frac{S}{V}Re^{2/3}Sc^{1/3}, \tag{31}$$

where S and V are the interior surface area and the volume of the chamber, respectively.

Note that this mass transfer correlation indicated in Eq. (30) is only applicable for evaluating particle deposition rate in the diffusional regime (e.g., $d_p < 0.1$ μm) in small cylindrical or spherical vessels with smooth surfaces, assuming that Re can be defined as stated in Eq. (30). For larger particles and higher fluid turbulence, deviations from Eq. (30) were observed because diffusion was no longer the only mechanism for deposition and other processes, such as inertial drift, may contribute to particle transport to the surfaces.

8. Summary

The phenomenon of particle deposition onto surfaces in a confined environment is frequently encountered in numerous industrial and environmental settings, either as a desirable or an undesirable outcome. This report presented a literature review on the important physical factors that influence particle deposition in enclosures, as well as the available experimental techniques and modeling approaches used for characterizing the rate of particle deposition. Experimental findings compared with the model calculations were presented, and the caveats with respect to the models were discussed.

As was already known, and is further substantiated by the scientific evidence presented here, the process of particle deposition is a complicated phenomenon. Transport behavior of particles to surfaces is governed by the nature of airflow near surfaces, including the turbulence intensity, the surface characteristics, and, importantly, particle size. The experimental studies reviewed in this report have revealed that the deposition rate varies broadly across conditions, and the measurement results are affected by various factors acting simultaneously. Direct measurements of particle deposition onto surfaces of interest are a challenging task to perform, and the contribution from various potential deposition mechanisms under realistic circumstances makes modeling work difficult. Nevertheless, further progress to elucidate the processes of particle deposition will require continued efforts to conduct more carefully controlled experimental investigations, in which the particle size, near-surface air flow conditions, and the nature of surfaces are well characterized.

9. Appendix

Table A1. Summary of Experimental Investigations Pertaining to Particle Deposition Measurements in Enclosed Environments

Investigators	Particle diameter	Particle composition	Test chamber	Aerosol analysis method	Flow conditions	Key findings
Langstroth and Gillespie, 1947[52]	0.6 to 4 μm	ammonium chloride	1.12 m^3 cube	electrostatic and thermal precipitation	natural convection and turbulent mixing	- The logarithm of the aerosol mass concentration was found to decrease linearly with time due to deposition to chamber surfaces. - The rate of particle deposition showed dependence on turbulent flow conditions.
Lieberman and Rosinski, 1962[66]	polydisperse 1 to 8 μm	zinc cadmium sulfide	310-L Lucite sphere	optical particle counter	natural convective mixing	- The presence of electric charges on poor conducting surface (e.g., plastic) can introduce additional variability in particle deposition measurements.
Van de Vate, 1972 [8]	0.09 to 1.3 μm	polystyrene latex particles (PSL)	1 m^3 (height = 2 m, S/V = 7 m^{-1})	electrostatic precipitation and microscopy	natural convective mixing	- The particle boundary layer thickness (0.85 mm) was estimated from the particle concentration decay measurements, assuming aerosols were deposited by gravity and diffusion only.
Harrison, 1979[82]	monodisperse 0.234 to 2.02 μm	polystyrene latex particles	58 × 58 ×58 cm^3 plywood chamber	light scattering particle counter	natural convective mixing	- Particle deposition rates were found to depend on the surface roughness (rough latex paint vs. smooth aluminum foil surface) - Particle concentration boundary layer thickness was found to be functions of particle size and surface roughness
Crump *et al.*, 1983[71]	monodisperse 0.024 to 0.794 μm	NaCl and polystyrene latex particles	roughly spherical glass vessel with a volume of 118 L	electrical aerosol analyzer for particle < 0.2 μm and optical particle counter for larger particles	turbulent mixing (continuous flow)	- The dependence of deposition rates on particle size and turbulent intensity were shown to agree well with the theoretical derivations by Crump and Seinfeld [68]. - A single value of turbulence parameter $k_e^{\ddagger}$ provided a moderately good fit to the measurement results for 0.02-0.8 μm particles.

Bigu, 1985[83]		radon and thoron progeny attached to airborne particles	26 m^3 test facility	plate-out experiments followed by α-activity measurements	turbulent and natural convective mixing	- The measured deposition velocities for Rn and Th progenies with the fan on (turbulent mixing) were significant higher than those measured with the fan off (convective mixing).
McMurry and Rader, 1985[67]	monodisperse 0.02-1.8 μm	NaCl	250 L Teflon film bag and 60 m^3 Teflon film smog chamber	condensation nucleus counter (CNC)	natural convective mixing	- Gravitational setting is the predominant particle loss mechanism for particles > 1 μm. - Brownian and turbulent diffusion is the dominant mechanism for removing particles < 0.05 μm. - Electrical forces were shown to contribute particle deposition significantly for smaller charged particles (0.05-1 μm), depending on the field strength near the surface. - Positive and negative particles were lost to the surface at the same rate when electrical force was the dominant transport mechanism.
Okuyama *et al.*, 1986[23]	monodisperse 0.006 to 2 μm	NaCl, diethylhexyl sebacate (DEHS), and polystyrene latex particles	cylindrical tank with a volume of 2.6 L; acrylic resin interior	light scattering particle counter for particles > 0.5 μm; particle size magnifier and light scattering particle counter for particles < 0.5 μm	turbulent mixing and no mixing	- No difference in deposition rate due to particle materials - Enhanced deposition rates were observed with increasing fluid turbulent intensity - Particle deposition rates exhibit a strong function of particle size with minimum deposition rate at 0.2 (no mixing) to 0.6 μm (vigorous mixing) - Good agreements between model and experiments were obtained for 0.006-0.2 μm particles, and for $k_e > \sim 10\ s^{-1}$. - Diffusion boundary layer thickness increases proportionally with $1/3^{th}$ power of Brownian diffusion coefficient.
Shimada *et al.*, 1987[60]	monodisperse 0.01 to 0.2 μm	NaCl, diethylhexyl sebacate (DEHS)	2.6-L cylindrical tank with sand-roughened interior walls	CNC	turbulent mixing	- Enhanced particle deposition onto rough surfaces was found compared to that onto smooth surfaces. - The enhancement of particle deposition, caused by turbulent diffusion very close to the surface, was more pronounced with increasing turbulent intensity and particle size.

Shimada *et al.*, 1988[62]	monodisperse 0.01 to 0.2 μm	NaCl, diethyl-hexyl sebacate (DEHS)	2.6-L cylindrical tank with interior walls lined with various roughness elements	CNC	turbulent mixing	- The effect of deposition rate enhancements due to surface roughness showed good agreements with the model predictions. - Increased particle depositions were observed with increasing particle size, stirring speed, and surface roughness.
Holub *et al.*, 1988[73]	0.001-0.3 μm	radon progeny attached to airborne particles	spherical glass chamber (BOM), 0.23 m^3; cylindrical chamber (SUG-NPL), 3.9 m^3	diffusion battery, CNC	natural convection (BOM); turbulent mixing by fan (SUG-NPL)	- The higher turbulence intensity in the SUG-NPL vessel played a role in the greater deposition rate measured for the unattached Rn than that in the BOM chamber by a factor of ~30. - The experimentally determined deposition rates in both chambers agreed with modeling predictions (Crump and Seinfeld [68]) with $n = 2.61$.
Shimada *et al.*, 1989 [5]	monodisperse 0.1 to 2 μm	polystyrene latex particles	cylindrical chamber, 3.9 m^3	optical particle counter and CNC	turbulent mixing by fan	- The effect of inertia on enhanced deposition rates was found for particles > 0.2 μm. - The particle deposition rates were shown to depend on turbulent intensities and particle sizes, with the minimum deposition rates for 0.3-0.5 μm particles. - The enhancement of particle deposition rates due to inertia was satisfactorily explained by the model by Schmel [84].
Shimada *et al.*, 1989[69]	charged and uncharged monodisperse 0.02-0.2 μm	NaCl	two cylindrical metal chambers with volumes 2.65 L and 0.57 L	CNC	turbulent mixing by impeller	- For charged and uncharged particles, no differences in measured deposition rates were found when the chamber walls were grounded. - Deposition rates of charged particles were significantly enhanced as the electric field strength increased, or as the particle size decreased. - The deposition rates could be reasonably predicted by taking into account Brownian/turbulent diffusion, and Coulombic forces acting on the particles.
Van Dingenen *et al.*, 1989[57]	monodisperse 0.02, 0.024, 0.03, 0.05, 0.1, 0.2 μm	NaCl	spherical borosilicate glass with a volume of 230 L	condensation nucleus counter (CNC)	natural convective mixing	- The observed particle deposition coefficients agreed with Crump and Seinfeld [68] taking n = 2.6. - Re-evaluation of experimental data from literature indicated that an appropriate value of k_e was

						the most important factor in determining particle deposition rates, while the exact value of n is of minor importance.
Chen *et al.*, 1992[42]	monodisperse 0.04-3 μm (0.04, 0.073, 0.215, 0.305, 0.481, 0.62, 0.76, 0.91, 1.09, 1.74, 2.02, 2.99)	PSL	Pyrex glass cylindrical chamber, 165 L	CNC and APS	natural convective mixing	- Minimum deposition loss was observed for 0.2-0.3 μm particles. - The flow turbulence intensity increased in the presence of temperature gradient, resulting in higher deposition rates for particles smaller than 1 μm. - The best fit of data and Crump and Seinfeld's model [68] occurred when $n = 2$.
Fotou and Pratsinis, 1993[85]	monodisperse 0.01-0.2 μm	NaCl	50-L glass spherical and 50-L polyethylene cylindrical vessels	CNC	turbulent mixing (continuous flow)	- The experimental data agreed with the mass transfer correlation by Pandian and Friedlander [74] as well as the model by Crump and Seinfeld [68].
Byrne *et al.*, 1995[49]	0.7, 2.5, 4.5, 5.4 μm	labeled with dysprosium (^{164}Dy) and indium (^{113}In)	$2 \times 2 \times 2$ m^3; aluminum surface	neutron activation analysis (NAA) for airborne particles collected on filters and deposited particles on surfaces	turbulent mixing by fan	- The measured particle deposition flux on floor, wall, and ceiling surfaces compared well with particle deposition velocities estimated by the concentration decay method. - Enhanced particle deposition flux was observed with surfaces of increasing roughness.
Morawska and Jamriska, 1996[86]	0.006 to 0.35 μm	radon progeny attached to airborne particles	cubical chamber with a volume of 3 m^3 (S = 12.5 m^2)	diffusion battery for Rn progeny, and differential mobility particle sizer for all airborne particles	natural convective mixing	- Particle deposition rates exhibited a minimum for particles between 0.1 to 0.25 μm, increased significantly for smaller particles, and slightly for larger particles.
Thatcher *et al.*, 1996[46]	0.1, 0.5, 0.7, 1.3, 2.5 μm	ammonium fluorescein	$1.22 \times 1.22 \times 1.22$ m^3; aluminum chamber	optical particle counter and filter samples for airborne particles; surface extraction followed by fluorometric analysis for deposited particles	natural convective mixing	- For horizontal surfaces, gravity played a dominant role in particle deposition for particles > 0.1 μm at ±1.5K (surface-to-air temperature difference); at ±10K, thermophoresis was important for submicron particles, but not significant for supermicron particles. - For vertical surfaces, gravity, inertia, and thermophoresis affect deposition velocity and the relative importance varies with particle size and

						surface-to-air temperature difference. - Non-uniform particle deposition was observed along the vertical surfaces.
Thatcher and Nazaroff, 1997 [7]	0.1, 0.5, 1.3 μm	ammonium fluorescein	1.22 × 1.22 × 1.22 m^3; aluminum chamber	optical particle counter and filter samples for airborne particles; surface extraction followed by fluorometric analysis for deposited particles	natural convective mixing	- Deposition of small particles (0.1 and 0.2 μm) was relatively insensitive to surface textures; increased deposition onto rough surfaces was found with particle size. - The surface roughness effect on particle deposition was greater for vertical surfaces than horizontal, and for warm surfaces than cool. - Particle deposition rates were influenced by surface roughness, surface orientation, surface-to-air temperature difference, and particle size.
Cheng, 1997[56]	monodisperse 0.005-0.14 μm for silver and 0.1-2 μm for polystyrene latex particles	silver and polystyrene latex particles	161-L spherical aluminum chamber	CNC for submicron particles and Aerodynamic Particle Sizer (APS) for supermicron particles	turbulent mixing (impeller) and no mixing	- Diffusional deposition and gravitational settling were dominant deposition mechanisms for particles < 0.1 μm and > 0.5 μm, respectively. - Increased turbulence was observed to enhance diffusional deposition, but not for particles > 1 μm when gravitational settling was the dominant mechanism. - The experimental data suggested that n = 2.6-2.8 yielded the best fit
Nomura *et al.*, 1997[54]	monodisperse 0.02 - 2 μm	soot, NaCl, carnauba wax, oil, and fluorescein particles	0.75 × 0.75 ×1.8 m^3 (S/V = 6.44 m^{-1})	CNC for < 1 μm and OPC (optical particle counter) for > 1 μm	turbulent mixing by continuous flow input	- Particle deposition rates were observed to depend on particle size and air-exchange rate (i.e., air turbulence intensity).
Abadie *et al.*, 2001[61]	monodisperse 0.7, 1, and 5 μm	polystyrene latex and dry powder	0.6 × 0.6 ×0.6 m^3	optical particle counter	turbulent mixing by a fan	- Significantly higher deposition rates onto rough surfaces (e.g., carpet) were measured than those onto smooth surfaces (e.g., linoleum).
Lai *et al.*, 2002[63]	monodisperse 0.7, 2.5, 4.5, 5.4 μm	labeled with dysprosium (^{164}Dy) and indium (^{113}In)	2 × 2 ×2 m^3; aluminum surface	neutron activation analysis (NAA) for airborne particles collected on filters and deposited particles on surfaces	turbulent mixing	- The ratio of particle deposition on rough surfaces relative to smooth surfaces increased with particle size and the level of air turbulence.

Thatcher *et al.*, 2002[64]	polydisperse 0.5-10 μm	olive oil	2.2×2.7 ×2.4 m^3	Aerodynamic Particle Sizer (APS)	natural convection and turbulent mixing by a fan	- Increased air mixing speed, surface roughness as well as surface area resulted in enhanced particle deposition rate. - Submicron particles exhibited more marked increase of deposition rates as a result of the furnishing level than supermicron particles.
Lai and Nazaroff, 2005[48]	monodisperse 0.9, 1.6, 2.2, 3.5, 5.0, 7.0, 7.8, 9.1 μm	ammonium fluorescein	1.22 × 1.22 × 1.22 m^3; aluminum chamber	optical particle counter and filter samples for airborne particles; surface extraction followed by fluorometric analysis for deposited particles	turbulent mixing	- Deposition velocities on smooth and rough vertical surfaces were determined for particles 0.9-9.1 μm. - The measured deposition velocity increases as particle size increases. - The measured deposition velocity increased with increasing roughness scale. - Particle size has more pronounced effects over surface roughness on deposition.
Lai, 2006[70]	monodisperse 3.5-9 μm	ammonium fluorescein	1.22 × 1.22 × 1.22 m^3; aluminum chamber	optical particle counter and filter samples for airborne particles; surface extraction followed by fluorometric analysis for deposited particles	turbulent mixing	- Due to electrostatic effects, the measured deposition velocities onto acetate sheets were higher by more than an order of magnitude than those onto glass surfaces. - Particle deposition can be significantly reduced by applying anti-electrostatic spray by 93% for acetate sheets and 68% for glass surfaces.

‡ k_ε : the turbulence intensity parameter; see discussions in Section 7.1.

10. References

1. D. W. Cooper, "Particulate Contamination and Microelectronics Manufacturing: An Introduction," *Aerosol Sci. Technol.* **5**, 287 (1986).

2. B. Y. H. Liu and K. H. Ahn, "Particle Deposition on Semiconductor Wafers," *Aerosol Sci. Technol.* **6**, 215 (1987).

3. S. E. Pratsinis, T. T. Kodas, M. P. Dudukovic, and S. K. Friedlander, "Aerosol Reactor Design: Effect of Reactor Type and Process Parameters on Product Aerosol Characteristics," *Ind. Eng. Chem. Process Des. Dev.* **25**, 634 (1986).

4. J. D. Spengler and K. Sexton, "Indoor Air Pollution: A Public Health Perspective," *Science* **221**, 9 (1983).

5. A. V. Nero, "Controlling Indoor Air Pollution," *Scientific American* **258**, 42 (1988).

6. W. W. Nazaroff, A. J. Gadgil, and C. J. Weschler, "Critique of the Use of Deposition Velocity in Modeling Indoor Air Quality," in *Modeling of Indoor Air Quality and Exposure, ASTM STP 1205*, N. L. Nagda, Ed., ASTM, Philadelphia, 81-104 (1993).

7. W. W. Nazaroff and G. R. Cass, "Protecting Museum Collections from Soiling Due to the Deposition of Airborne Particles," *Atmospheric Environ.* **25A**, 841 (1991).

8. A. Wright, "Primary System Fission Product Transport and Release," Report NUREG/CR-6193, ORNL/TM-12681, Oak Ridge National Laboratory, Oak Ridge, TN (1994).

9. F. Gelbard, "Maeros User Manual," U.S. Nuclear Regulatory Commission, Washington, DC (1982).

10. F. E. Kruis, H. Fissan, and A. Peled, "Synthesis of Nanoparticles in the Gas Phase for Electronic, Optical, and Magnetic Applications - A Review," *J. Aerosol Sci.* **29**, 511 (1998).

11. T. T. Kodas, "Generation of Complex Metal Oxides by Aerosol Processes: Superconducting Ceramic Particles and Films," *Adv. Mater.* **1**, 180 (1989).

12. A. C. Tribble, *Fundamentals of Contamination Control*, SPIE Press, Bellingham, WA (2000).

13. B. Y. H. Liu and K. W. Lee, "Experimental Study of Aerosol Filtration by Fibrous Filters," *Aerosol Sci. Technol.* **1**, 35 (1981).

14. L. Spielman and S. L. Goren, "Model for Predicting Pressure Drop and Filtration Efficiency in Fibrous Media," *Environ. Sci. Technol.* **2**, 279 (1968).

15. M. R. Sippola, "Particle Deposition in Ventilation Ducts," Ph.D. dissertation, University of California at Berkeley, Berkeley, CA (2002).

16. P. G. Papavergos and A. B. Hedley, "Particle Deposition Behavior from Turbulent Flows," *Chemical Engineering Research and Design* **62**, 275 (1984).

17. F. Schmidt, K. Gartz and H. Fissan, "Turbulent Particle Deposition on a Horizontal Circular Plate," *J. Aerosol Sci.* **28**, 973 (1997).

18. Y. Ye, D. Y. H. Pui, B. Y. H. Liu, S. Opiolka, S. Blumhorst, and H. Fissan, "Thermophoretic Effect of Particle Deposition on a Free-Standing Semiconductor Wafer in a Clean Room," *J. Aerosol Sci.* **22**, 63 (1991).

19. Y. Otani, H. Emi, C. Kanaoka, and K. Kato, "Determination of Deposition Velocity onto a Wafer for Particles in the Size Range between 0.3 and 0.8 μm," *J. Aerosol Sci.* **20**, 787 (1989).

20. N. A. Fuchs, *The Mechanics of Aerosols*, Pergamom Press, Oxford (1964).

21. J. F. Van De Vate, "Investigations into the Dynamics of Aerosols in Enclosures as Used for Air Pollution Studies," Report ECN-86, Netherlands Energy Research Foundation (1980).

22. W. W. Nazaroff, M. P. Logocki, T. Ma, and G. R. Cass, "Particle Deposition in Museums: Comparison of Modeling and Measurement Results," *Aerosol Sci. Technol.* **13**, 332 (1990).

23. K. Okuyama, Y. Kousaka, S. Yamamoto, and T. Hosokawa, "Particle Loss of Aerosols with Particle Diameters between 6 and 2000 nm in Stirred Tank," *J. Colloid Interface Sci.* **110**, 214 (1986).

24. W. W. Nazaroff and G. R. Cass, "Particle Deposition from a Natural Convection Flow onto a Vertical Isothermal Flat Plate," *J. Aerosol Sci.* **18**, 445 (1987).

25. A. C. K. Lai and W. W. Nazaroff, "Modeling Indoor Particle Deposition from Turbulent Flow onto Smooth Surfaces," *J. Aerosol Sci.* **31**, 463 (2000).

26. A. Bejan, *Convective Heat Transfer*, John Wiley and Sons, New York (1984).

27. S. K. Friedlander, *Smoke, Dust, and Haze: Fundamentals of Aerosol Dynamics*, 2nd ed., Oxford University Press, Oxford (2000).

28. W. C. Hinds, *Aerosol Technology: Properties, Behavior, and Measurement of Airborne Particles*, 2nd ed., John Wiley and Sons, New York (1999).

29. J. O. Hinze, *Turbulence*, McGraw-Hill, New York (1975).

30. W. Uijttewaal, "Particle Motion in Turbulent Pipe Flow," Report MEAH-128 TU Delft Lab for Aero- and Hydrodynamics, Delft University of Technology, Delft, The Netherlands (1995).

31. J. H. Seinfeld and S. N. Pandis, *Atmospheric Chemistry and Physics*, 2nd ed., John Wiley and Sons, New York, (1998).

32. J. Aitken, "On the Formation of Small Clear Spaces in Dusty Air," *Trans. Roy. Soc. Edinburgh* **32**, 239 (1884).

33. H. H. Watson, "The Dust-Free Space Surrounding Hot Bodies," *Trans. Faraday Soc.* **32**, 1073 (1936).

34. W. Zernik, "The Dust-Free Space Surrounding Hot Bodies," *Brit. J. Appl. Phys.* **8**, 117 (1957).

35. L. Talbot, R. K. Cheng, R. W. Schefer, and D. R. Willis, "Thermophoresis of Particles in a Heated Boundary Layer," *J. Fluid Mech.* **101**, 737 (1980).

36. A. Li and G. Ahmadi, "Aerosol Particle Deposition with Electrostatic Attraction in a Turbulent Channel Flow," *J. Colloid Interface Sci.* **158**, 476 (1993).

37. M. Caporaloni, F. Tampieri, F. Trombetti, and O. Vittori, "Transfer of Particles in Nonisotropic Air Turbulence," *J. Atmos. Sci.* **32**, 565 (1975).

38. M. W. Reeks, "The Transport of Discrete Particles in Inhomogeneous Turbulence," *J. Aerosol Sci.* **14**, 729 (1983).

39. S. T. Johansen, "The Deposition of Particles on Vertical Walls," *Int. J. Multiphase Flow* **17**, 355 (1991).

40. A. Guha, "A Unified Eulerian Theory of Turbulent Deposition to Smooth and Rough Surfaces," *J. Aerosol Sci.* **28**, 1517 (1997).

41. J. Young and A. Leeming, "A Theory of Particle Deposition in Turbulent Pipe Flow," *J. Fluid Mech.* **340**, 129 (1997).

42. B. T. Chen, H. C. Yeh and Y. S. Cheng, "Evaluation of an Environmental Reaction Chamber ," *Aerosol Sci. Technol.* **17**, 9 (1992).

43. P. A. Baron and K. Willeke, *Aerosol Measurements: Principles, Techniques, and Applications*, 2nd ed., John Wiley and Sons, New York (2001).

44. P. H. McMurry, "A Review of Atmospheric Aerosol Measurements," *Atmospheric Environ.* **34**, 1959 (2000).

45. S. K. Friedlander and H. F. Johnstone, "Deposition of Suspended Particles from Turbulent Gas Streams," *Ind. Eng. Chem.* **49**, 1151 (1957).

46. T. L. Thatcher, W. A. Fairchild, and W. W. Nazaroff, "Particle Deposition from Natural Convection Enclosure Flow onto Smooth Surfaces," *Aerosol Sci. Technol.* **25**, 359 (1996).

47. T. L. Thatcher and W. W. Nazaroff, "Effects of Small-Scale Obstructions and Surface Textures on Particle Deposition from Natural Convection Flow," *Aerosol Sci. Technol.* **27**, 709 (1997).

48. A. C. K. Lai and W. W. Nazaroff, "Supermicron Particle Deposition from Turbulent Chamber Flow onto Smooth and Rough Vertical Surfaces," *Atmospheric Environ.* **39**, 4893 (2005).

49. M. A. Byrne, A. J. H. Goddard, C. Lange, and J. Roed, "Stable Tracer Aerosol Deposition Measurements in a Test Chamber," *J. Aerosol Sci.* **26**, 645 (1995).

50. A. C. K. Lai, M. A. Byrne, and A. J. H. Goddard, "Measured Deposition of Aerosol Particles on a Two-Dimensional Ribbed Surface in a Turbulent Duct Flow," *J. Aerosol Sci.* **30**, 1201 (1999).

51. A. C. K. Lai, M. A. Byrne, and A. J. H. Goddard, "Aerosol Deposition in Turbulent Channel Flow on a Regular Array of Three-Dimensional Roughness Elements," *J. Aerosol Sci.* **32**, 121 (2001).

52. G. O. Langstroth and T. Gillespie, "Coagulation and Surface Losses in Disperse Systems in Still and Turbulent Air," *Canad. J. Chem.* **25**, 455 (1947).

53. J. Corner and E. D. Pendlebury, "The Coagulation and Deposition of a Stirred Aerosol," *Proc. Phys. Soc. London, Sect. B*, **B64**, 645 (1951).

54. Y. Nomura, P. K. Hopke, B. Fitzgerald, and B. Mesbah, "Deposition of Particles in a Chamber as a Function of Ventilation Rate," *Aerosol Sci. Technol.* **27**, 62 (1997).

55. M. Shimada, K. Okuyama, and Y. Kousaka, "Influence of Particle Inertia on Aerosol Deposition in a Stirred Turbulent Flow Field," *J. Aerosol Sci.* **20**, 419 (1989).

56. Y. S. Cheng, "Wall Deposition of Radon Progeny and Particles in a Spherical Chamber," *Aerosol Sci. Technol.* **27**, 131 (1997).

57. R. Van Dingenen, F. Raes, and H. Vanmarcke, "Molecule and Aerosol Particle Wall Losses in Smog Chambers Made of Glass," *J. Aerosol Sci.* **20**, 113 (1989).

58. J. F. Van De Vate, "The Thickness of the Stagnant Air Layer in Aerosol Containments and the Aerodynamic Diameter of Aggregates of Small Spheres," *J. Colloid Interface Sci.* **41**, 194 (1972).

59. A. D. Zimon, *Adhesion of Dust and Powder*, 2nd ed., Consultants Bureau, New York (1982).

60. M. Shimada, K. Okuyama, Y. Kousaka, and K. Ohshima, "Turbulent and Brownian Diffusive Deposition of Aerosol Particles onto a Rough Wall," *J. Chem. Eng. Japan* **20**, 57 (1987).

61. M. Abadie, K. Limam, and F. Allard, "Indoor Particle Pollution: Effect of Wall Textures on Particle Deposition," *Building Environ.* **36**, 821 (2001).

62. M. Shimada, K. Okuyama, Y. Kousaka, and J. H. Seinfeld, "A Model Calculation of Particle Deposition onto Rough Wall by Brownian and Turbulent Diffusion," *J. Colloid Interface Sci.* **125**, 198 (1988).

63. A. C. K. Lai, M. A. Byrne, and A. J. H. Goddard, "Experimental Studies of the Effect of Rough Surfaces and Air Speed on Aerosol Deposition in a Test Chamber," *Aerosol Sci. Technol.* **36**, 973 (2002).

64. T. L. Thatcher, A. C. K. Lai, R. Moreno-Jackson, R. G. Sextro, and W. W. Nazaroff, "Effects of Room Furnishings and Air Speed on Particle Deposition Rates Indoors," *Atmospheric Environ.* **36**, 1811 (2002).

65. W. W. Nazaroff and G. R. Cass, "Mass-Transport Aspects of Pollutant Removal at Indoor Surfaces," *Environ. Int.* **15**, 567 (1989).

66. A. Lieberman and J. Rosinski, "Behavior of an Aerosol Cloud in a Plastic Chamber," *J. Colloid Interface Sci.* **17**, 814 (1962).

67. P. H. McMurry and D. J. Rader, "Aerosol Wall Losses in Electrically Charged Chambers," *Aerosol Sci. Technol.* **4**, 249 (1985).

68. J. G. Crump and J. H. Seinfeld, "Turbulent Deposition and Gravitational Sedimentation of an Aerosol in a Vessel of Arbitrary Shape," *J. Aerosol Sci.* **12**, 405 (1981).

69. M. Shimada, K. Okuyama, Y. Kousaka, Y. Okuyama, and J. H. Seinfeld, "Enhancement of Brownian and Turbulent Diffusive Deposition of Charged Particles in the Presence of Electric Field," *J. Colloid Interface Sci.* **128**, 157 (1989).

70. A. C. K. Lai, "Investigation of Electrostatic Forces on Particle Deposition in a Test Chamber," *Indoor Built Environ.* **15**, 179 (2006).

71. J. G. Crump, R. C. Flagan, and J. H. Seinfeld, "Particle Wall Loss Rates in Vessels," *Aerosol Sci. Technol.* **2**, 303 (1983).

72. K. Okuyama, Y. Kousaka, Y. Kida, and T. Yoshida, "Turbulent Coagulation of Aerosols in a Stirred Tank," *J. Chem. Eng. Japan* **10**, 142 (1977).

73. R. F. Holub, F. Raes, R. Van Dingenen, and H. Vanmarcke, "Deposiiton of Aerosols and Unattached Radon Daughters in Different Chambers; Theory and Experiment," *Rad. Protec. Dosi.* **24**, 217 (1988).

74. M. D. Pandian and S. K. Friedlander, "Particle Deposition to Smooth and Rough Walls of Stirred Chambers: Mechanisms and Engineering Correlations," *Physicochem. Hydrodynam.* **10**, 639 (1988).

75. M. Beneš and R. F. Holub, "Aerosol Wall Deposition in Enclosures Investigated by Means of a Stagnant Layer," *Environ. Int.* **22, Suppl. 1**, S883 (1996).

76. H. Schlichting, *Boundary-Layer Theory*, 7th ed., McGraw-Hill, New York (1979).

77. H. H. Brunn, *Hot-Wire Anemometry: Principles and Signal Analysis*, Oxford University Press, Oxford (1995).

78. A. C. K. Lai, "Modeling Indoor Coarse Particle Deposition onto Smooth and Rough Vertical Surfaces," *Atmospheric Environ.* **39**, 3823 (2005).

79. N. B. Wood, "A Simple Method for the Calculation of Turbulent Deposition to Smooth and Rough Surfaces," *J. Aerosol Sci.* **12**, 275 (1981).

80. F. Chen and A. C. K. Lai, "An Eulerian Model for Particle Deposition under Electrostatic and Turbulent Conditions," *J. Aerosol Sci.* **35**, 47 (2004).

81. R. B. Bird, W. E. Stewart, and E. N. Lightfoot, *Transport Phenomena*, John Wiley and Sons, New York (1960).

82. A. W. Harrison, "Quiescent Boundary Layer Thickness in Aerosol Enclosures under Convective Stirring Conditions," *J. Colloid Interface Sci.* **69**, 563 (1979).

83. J. Bigu, "Radon Daughter and Thoron Daughter Deposition Velocity and Unattached Fraction under Laboratory-Controlled Conditions and in Underground Uranium Mines," *J. Aerosol Sci.* **16**, 157 (1985).

84. G. A. Sehmel, "Particle Deposition from Turbulent Air Flow ," *J. Geophysical Res* **75**, 1766 (1970).

85. G. P. Fotou and S. E. Pratsinis, "A Correlation for Particle Wall Losses by Diffusion in Dilution Chambers," *Aerosol Sci. Technol.* **18**, 213 (1993).

86. L. Morawska and M. Jamriska, "Deposition of Radon Progeny on Indoor Surfaces," *J. Aerosol Sci.* **27**, 305 (1996).

PHYSICAL SCIENCES LABORATORIES

The Aerospace Corporation functions as an "architect-engineer" for national security programs, specializing in advanced military space systems. The Corporation's Physical Sciences Laboratories support the effective and timely development and operation of national security systems through scientific research and the application of advanced technology. Vital to the success of the Corporation is the technical staff's wide-ranging expertise and its ability to stay abreast of new technological developments and program support issues associated with rapidly evolving space systems. Contributing capabilities are provided by these individual organizations:

Electronics and Photonics Laboratory: Microelectronics, VLSI reliability, failure analysis, solid-state device physics, compound semiconductors, radiation effects, infrared and CCD detector devices, data storage and display technologies; lasers and electro-optics, solid-state laser design, micro-optics, optical communications, and fiber-optic sensors; atomic frequency standards, applied laser spectroscopy, laser chemistry, atmospheric propagation and beam control, LIDAR/LADAR remote sensing; solar cell and array testing and evaluation, battery electrochemistry, battery testing and evaluation.

Space Materials Laboratory: Evaluation and characterizations of new materials and processing techniques: metals, alloys, ceramics, polymers, thin films, and composites; development of advanced deposition processes; nondestructive evaluation, component failure analysis and reliability; structural mechanics, fracture mechanics, and stress corrosion; analysis and evaluation of materials at cryogenic and elevated temperatures; launch vehicle fluid mechanics, heat transfer and flight dynamics; aerothermodynamics; chemical and electric propulsion; environmental chemistry; combustion processes; space environment effects on materials, hardening and vulnerability assessment; contamination, thermal and structural control; lubrication and surface phenomena. Microelectromechanical systems (MEMS) for space applications; laser micromachining; laser-surface physical and chemical interactions; micropropulsion; micro- and nanosatellite mission analysis; intelligent microinstruments for monitoring space and launch system environments.

Space Science Applications Laboratory: Magnetospheric, auroral and cosmic-ray physics, wave-particle interactions, magnetospheric plasma waves; atmospheric and ionospheric physics, density and composition of the upper atmosphere, remote sensing using atmospheric radiation; solar physics, infrared astronomy, infrared signature analysis; infrared surveillance, imaging and remote sensing; multispectral and hyperspectral sensor development; data analysis and algorithm development; applications of multispectral and hyperspectral imagery to defense, civil space, commercial, and environmental missions; effects of solar activity, magnetic storms and nuclear explosions on the Earth's atmosphere, ionosphere and magnetosphere; effects of electromagnetic and particulate radiations on space systems; space instrumentation, design, fabrication and test; environmental chemistry, trace detection; atmospheric chemical reactions, atmospheric optics, light scattering, state-specific chemical reactions, and radiative signatures of missile plumes.

The Aerospace Corporation
2310 E. El Segundo Boulevard
El Segundo, California 90245-4609
U.S.A.